Review

Alina Karabchevsky*, Aviad Katiyi, Angeleene S. Ang and Adir Hazan

On-chip nanophotonics and future challenges

https://doi.org/10.1515/nanoph-2020-0204
Received March 19, 2020; accepted June 2, 2020; published online July 13, 2020

Abstract: On-chip nanophotonic devices are a class of devices capable of controlling light on a chip to realize performance advantages over ordinary building blocks of integrated photonics. These ultra-fast and low-power nanoscale optoelectronic devices are aimed at high-performance computing, chemical, and biological sensing technologies, energy-efficient lighting, environmental monitoring and more. They are increasingly becoming an attractive building block in a variety of systems, which is attributed to their unique features of large evanescent field, compactness, and most importantly their ability to be configured according to the required application. This review summarizes recent advances of integrated nanophotonic devices and their demonstrated applications, including but not limited to, mid-infrared and overtone spectroscopy, all-optical processing on a chip, logic gates on a chip, and cryptography on a chip. The reviewed devices open up a new chapter in on-chip nanophotonics and enable the application of optical waveguides in a variety of optical systems, thus are aimed at accelerating the transition of nanophotonics from academia to the industry.

Keywords: deep-learning; overtone spectroscopy; parity-time; plasmonics; waveguide.

1 Introduction

The 21st century is the era of photonics and quantum optics after the 20th century which was considered as the era of electronics. The miniaturization of optoelectronic components is driven by the demand for ergonomic and fast information processing, sensing and others in a multiplicity of applications from cyber security, banking, healthcare, communications, defense, and non-destructive detection. The scale of miniaturization, low cost, and robustness of microfabrication approaches which have enabled the ubiquitous presence of the mobile phone and laptop are expected to lead to similarly widespread deployment of quantum and all-optical computers on a chip.

On-chip photonics or *Integrated photonics* is the branch of photonics in which planar dielectric waveguides are fabricated on a chip such as those summarized in Ref. [1]. *On-chip nanophotonics* is the emerging and rapidly growing branch of On-chip photonics in which the waveguides are either of nanoscale dimensions such as summarized in Ref. [2] or hybrid waveguides (composite waveguides) which are classical waveguides with nanoscale overlayers of slab film [3], nanoantennas [4, 5] or metamaterial overlayers [6–9]. In addition, *On-chip nanophotonics* allows for the design, fabrication, and integration of several nanophotonic components on a common substrate utilizing guided-wave optics principles. Setting up the on-chip nanophotonic technologies involves confluence of several disciplines dealing with light such as guided-wave optics, nanophotonics, plasmonics, silicon photonics, and waveguide technology.

Traditionally, optical waveguides, the basic element of photonic integrated circuitry (PIC), were mainly made from transparent glasses, reflective metals, and various optical thin films [10]. These bulk materials selectively refract and reflect light according to Snell's law, Fermat's principle, Fresnel's equations and Fresnel–Kirchhoff's diffraction formula [11]. The ever-growing interest in upgrading the performance of classical optical waveguides and overcoming the fundamental difficulties had to face several major challenges including surmounting the diffraction limit and other restrictions set by classical theories, and reducing the complexity and cost of photonic integrated circuits.

In the last decades, the manufacturing scale of optical waveguides was expanded into dimensions smaller than the wavelength and allowed exploiting the light scattered by subwavelength structures, in which the light propagation can be tuned almost arbitrarily [12, 13]. In addition, full-vectorial electromagnetic computational algorithms have facilitated the rigorous designs of complex structures

***Corresponding author: Alina Karabchevsky**, School of Electrical and Computer Engineering, Ben-Gurion University of the Negev, Beer-Sheva, 8410501, Israel, E-mail: alinak@bgu.ac.il. https://orcid.org/0000-0002-4338-349X
Aviad Katiyi, Angeleene S. Ang and Adir Hazan: School of Electrical and Computer Engineering, Ben-Gurion University of the Negev, Beer-Sheva, 8410501, Israel

Open Access. © 2020 Alina Karabchevsky et al., published by De Gruyter. This work is licensed under the Creative Commons Attribution 4.0 International License.

with multiscale characteristic dimensions [14]. Figure 1 shows the bar chart of publication records in field of on-chip nanophotonics (from Web of Science with key-words on-chip nanophotonics, waveguides) showing fast evolution growth of the field over the years beginning from 2000 until 2019.

At the nanoscale, subwavelength light–matter interaction is blended with classic and quantum effects in various functional materials used in on-chip photonics such as noble metals [15, 16], semiconductors [17], phase-change materials [18, 19], and 2D materials [20, 21]. These so-called metamaterials [22] provide unprecedented opportunities to upgrade the performance of classic optical devices. Metamaterials are artificial materials with subwavelength features. When used as a waveguide overlayer, they act as miniature anisotropic light scatterers. As a result, the phase, amplitude, and polarization of light can be engineered to provide the needed optical response on a chip.

Incorporation of metamaterials into on-chip photonic devices can tune the performance of a waveguide, such as reducing waveguide facet reflection losses with anti-reflective structures [23, 24], engineering the waveguide effective index to convert the propagating modes [25], and 'hiding carpet' cloaking an object on a chip [6]. Here, we overview the phenomena associated with the propagation and manipulation of light in dielectric waveguides, waveguides with plasmonic overlayer or metamaterials on waveguides.

In this paper, we present an updated review of the current developments in on-chip nanophotonics, identifying optical devices for emerging applications that need further optimization and suggesting opportunities where on-chip nanophotonic architectures can be uniquely valuable. The paper is structured as follows: Section 2 focuses on building blocks required for the design of on-chip nanophotonic devices, their architectures and spatial field distributions. The reviewed building blocks are discussed in Section 2.1 passive components and in Section 2.2 active components. Section 3 gives some suggestions for on-chip nanophotonics emerging applications such as the overtone spectroscopy on a chip in Section 3.1. In addition, we present the fundamental concepts and methods that were studied and used to explore subwavelength structuring in multi-layer systems on a chip and optical waveguides. We review the principles of field concentration and enhancement in plasmonic structures. We elaborate on the theory of wave propagation in different periodic media and present some of its applications in multi-layer structures and waveguides. Finally, we discuss the principles of sub wavelength structure materials and how they can be used to control electromagnetic fields on a chip. Section 4 focuses on major advances in on-chip quantum nanophotonics. Section 5 focuses on manipulation of light-on-a-chip with metasurface overlayers or nanoparticles. We explain the excitation of hybrid modes in dielectric and plasmonic overlayers on waveguides, and demonstrate how the evanescent field of such a device can be manipulated to create a novel functionality of a waveguide. We present the design and implementation of metasurfaces capable of converting the eigenmodes supported by a silicon waveguide from one to another, and metasurfaces which reduce waveguide coupling losses. Research activities where materials of subwavelength dimensions are utilized for the development of novel chip-scale devices are overviewed. In addition, the practical considerations for a novel surface plasmon resonance (SPR sensors) on a chip are presented. In Section 6, we summarize the current status of on-chip nanophotonic platform developments, highlight the remaining challenges and the unique opportunities that can be pursued using chip-scale platform, such as on-chip trapping schemes (in Section 6.1) and on-chip energy-conserving logical elements in Section 6.2.

2 On-chip photonics

The basic structure of on-chip photonics is the optical passive waveguide – a transparent dielectric structure

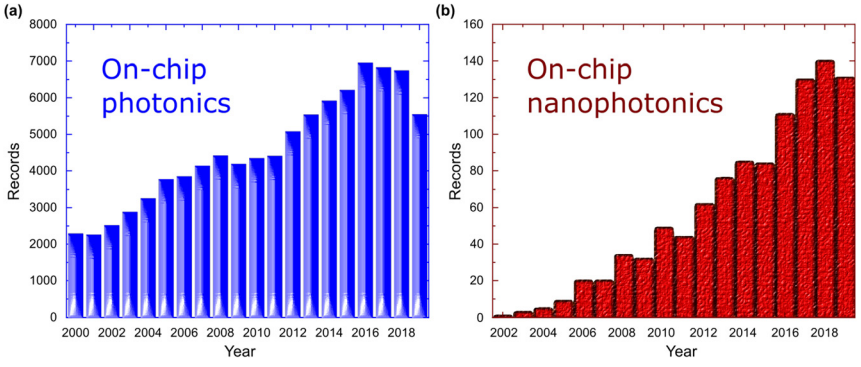

Figure 1: Evolution of on-chip nanophotonic devices over the years 2000–2019: (a) Bar chart of publication records in field of on-chip photonics and waveguides (from the Web of Science), (b) Bar chart of publication records in field of on-chip nanophotonics (from the Web of Science).

capable of confining and transporting energy, composed of a small cross-section – as illustrated in Figure 2a. The optical fiber is a waveguide of cylindrical geometry; the waveguides used in on-chip photonics are planar, composed of at least three layers: the substrate, the guiding layer (or core), and a cladding (air or others). The light is guided in the waveguide core due to the effect of total internal reflection (TIR) [11]. To learn on the wave propagation in each waveguide configuration, we refer the reader to the textbooks which elaborate on the theory of guided-wave optics such as Snyder and Love [26], Hunsperger [27], and Chrostowski and Hochberg [28].

2.1 Passive components

Common configurations of passive waveguides include [1] slab, strip loaded, ridge, rib, buried, and diffused, as schematically shown in Figure 2a. Each configuration has unique properties and can be utilized for different applications. Ridge waveguides are an excellent choice for sensing due to the good overlap with the superstrate. Buried waveguides are a good choice for optical signal transmission, similar to optical fibers, buried waveguide is covered by cladding. Light in a waveguide propagates as a discrete electromagnetic wave which is a solution of the wave equation for particular boundary conditions of the waveguide and materials. Discrete field distributions, named the *waveguide modes* [26]. Depending on the size and refractive index of the waveguide, it can support a single or several guided modes. Figure 2b shows numerical results of fundamental modes calculated for common passive waveguide architectures. Rib waveguide would be of larger dimensions to support the single-mode operation as compared to the ridge waveguide for which the coupling is easier. In addition, the mode has lower interaction with

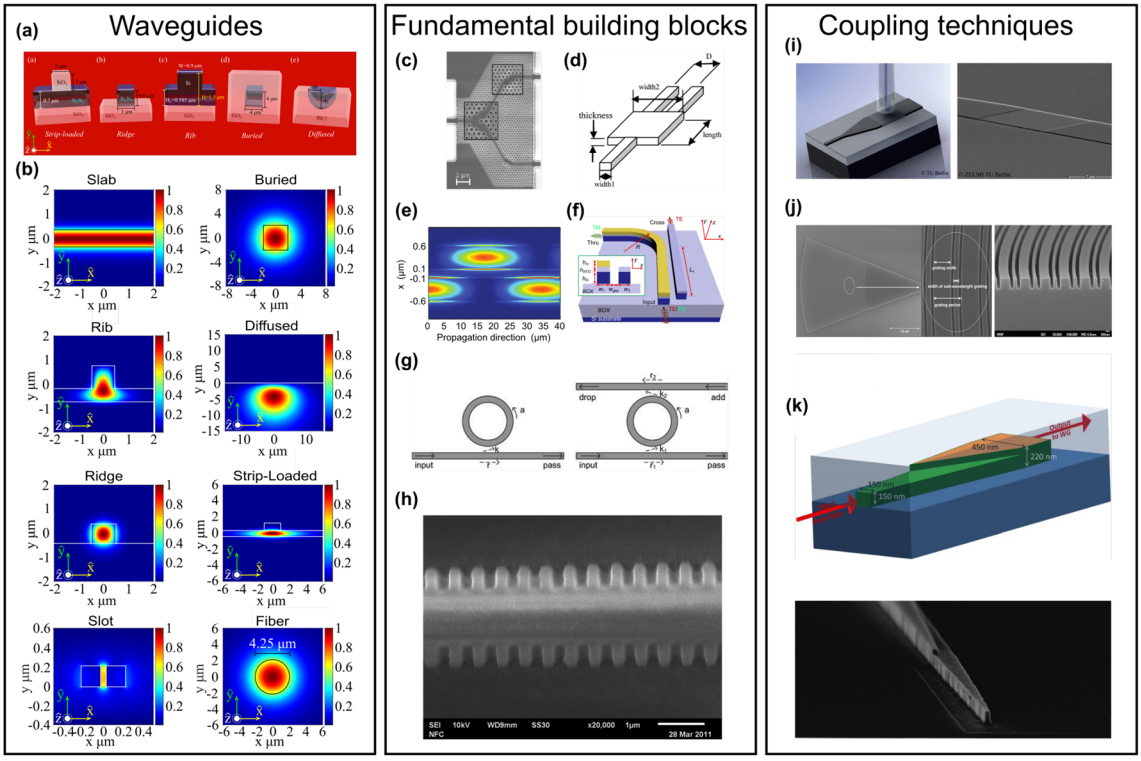

Figure 2: Key passive components in on-chip nanophotonics. (a) Rendered images of laterally confined common passive waveguide architectures (reproduced from [1]). (b) Quasi-TE polarization colormaps of $|E_x(x, y)|$, normalized to the maximum amplitude in monomode waveguides (reproduced from [1]): slab, buried, rib, diffused, ridge, strip-loaded, slot waveguide, and an optical fiber (reproduced from [1]). (c) Scanning electron micrograph (SEM) images of the fabricated photonic crystal waveguide (PhCW) splitter (reproduced from [29]). (d) The splitter schematic main parameters (reproduced from [30]). (e) Evolution field propagation along the directional coupler (reproduced from [28]). (f) Schematic configuration of the proposed polarization beam splitter (PBS) with the cross-section shown in the inset (reproduced from [31]). (g) All-pass and Add-drop ring resonators (reproduced from [32]). (h) Image of sidewall Bragg grating waveguide (BGW) (reproduced from [33]). (i) Out-of-plane coupling from fiber to waveguide using a grating coupler and SEM image of a grating coupler in a waveguide (reproduced from [34]). (j) SEM images of the focusing sub-wavelength grating coupler: a top and a sidewall views (reproduced from [35]). (k) Schematics of an on-chip Bilayer Inverse Taper (BIT) edge coupler and SEM micrograph of a fabricated BIT (reproduced from [36]).

the waveguide which makes the sidewall scattering lower. In ridge waveguides, a large fraction of the mode is beyond the guiding layer boundaries which makes the ridge waveguide preferred for evanescent field-based applications [1, 37]. The slot waveguides (Figure 2b) can be single-mode and highly confined in a small dimensions which cannot be achieved with other waveguide architectures. The mode propagates in the low-index medium which makes this configuration favorable for sensing [38].

It is important to note, that as a mode m propagates along a waveguide, a portion of the mode exists beyond the waveguide's physical dimensions and is named the *evanescent wave* (or field). Evanescent wave is non-propagating wave. Evanescent fields in waveguides can be evaluated by the *penetration depth* (d_p) of the field. *Penetration depth* is the distance from the waveguide surface, for which the intensity or power of the field decays to $1/e$ or about 37% of its surface value, defined as

$$d_p = \frac{\lambda}{2\pi\sqrt{n_2^2 \sin^2(\theta_i) - n_1^2}} \quad (1)$$

where n_2 and n_1 are refractive index of waveguide core and cladding respectively, θ_i is the incident angle to the normal of the interface between the waveguide core and the cladding. Evanescent field is a side effect of TIR and mathematically described as the exponential solution of the wave equation solved in Cartesian coordinates for planar waveguides (or second kind of modified Bessel functions for fibers, then the wave equation is solved in Cylindrical coordinates) [26]. For the fundamental mode (zero order mode $m = 0$), the V-number is very small ($h/\lambda \ll 1$) and the guided wave travels close to the critical angle (normalized effective index $b \ll 1$, $b = (N^2 - n_1^2)/(n_2^2 - n_1^2)$, $N = \beta/k$ with propagation constant β), then the effective index is close to that of the cladding. In this case, the wave penetrates deeply into the cladding (analyte or substrate) because the rays are near the critical angle and the evanescent decay is slow. For higher order modes, when the V-number $V = kh\sqrt{n_2^2 - n_1^2}$ increases, the ray travels nearly parallel to the waveguide axis and the effective refractive index would be close to the waveguide core index n_2. In this case, the wave in the cladding (analyte or substrate) will decay very rapidly for evanescent waves traveling at angles far above the critical angle.

The optical power *splitter* is an important component in on-chip photonics. It divides the input power (or splits polarization) into separate channels. One of the widely used waveguide splitter configuration is the Y-branch splitter, in which the guiding layer is separated into two branches. PhCW [29], as shown in Figure 2c, can also serve as a splitter. PhCW is reducing the dimensions of the splitter by up to 10^6 times [29]. Another splitter configuration is a compact 90° trench-based splitter [39] – the waveguide is designed such that there is a perpendicular branch attached to the waveguide, and a trench is etched near the intersection, which creates a beam splitter. A directional coupler can serve to split power [40]. However, for splitting the light into more than two branches, the multimode interference (MMI) effect can be utilized [41]. Due to the self-imaging effect in MMI waveguides, multiple images along the propagation direction are created. By choosing the proper structure length L, the input field can be divided to up to 16 branches. Moreover, MMI splitters have lower losses and shorter lengths compared to Y-splitters [42], but they are wavelength-specific. Splitters can also be designed to split polarization using hybrid plasmonic waveguides [36], as shown in Figure 2f.

The *directional coupler*, shown in Figure 2e (left), is a passive waveguide architecture that uses the evanescent field in order to transfer power between two waveguides. By tuning the distance between the waveguides, as well as the coupling length, it is possible also to tune the amount of power transferred between the waveguides. Either the entirety of the power can be transferred, or half, or a fraction, of the power, which makes it act as a power splitter. An on-chip component based on the directional coupler principles is the *ring resonator*. The ring resonator is a structure composed of a waveguide and a ring, as shown in Figure 2g. At the point where the ring and the waveguide are closest to each other (evanescently couple), the ring resonator acts like a directional coupler. The strong wavelength selectivity of this device allows it to serve as a narrow-band filter, used for a wide variety of applications, such as a light source [43, 44], modulator [45–47] and sensor [48, 49].

In on-chip photonics, there is also a need for combining and separating signals of multiple wavelengths. For this purpose, the *Bragg grating* structures can be used. Those structures have periodic pattern of effective index changes that etched on the waveguide, as shown in Figure 2h. These structures can be etched by UV laser and intense femtosecond pulses illumining the bulk glass [50] or fibers [51]. Since the Bragg grating is wavelength-specific, the grating can be used to selectively accept and/or filter out signals. It can act as a mirror, creating a narrow band laser [52]. In addition, due to the high sensitivity of the grating to its environment, the Bragg grating can be used in sensing applications, to detect changes in temperature [53], strain [53], or refractive index [54, 55].

The integrated photonic chip also needs to communicate with the outside world, in terms of input and output

ports. For this, an important parameter to consider when designing a waveguide is the *coupling efficiency* between the waveguide and the input or output optical fiber. One of the most popular coupling schemes is the butt-coupling scheme. However, a single-mode fiber operating at the telecommunication window has about 9 μm diameter core which leads to the large mismatch between the fiber mode shown in Figure 2b and a waveguide mode shown in Figure 2a. The modal mismatch described mathematically by the overlap integral between two modes, reduces the coupling efficiency, introducing the losses. Hence, improving the coupling efficiency is an essential topic in the on-chip nanophotonics.

In order to improve the coupling efficiency, a Bragg grating can be used [34], as shown in Figure 2i. For this, the grating parameters needs to fit the incident beam, then the waveguide is usually tapered (Figure 2i [right]), but this coupling configuration is long. The grating can be designed to focus the light, such that the overall configuration will be more compact [35], as shown in Figure 2j. The Bragg grating coupler is a single-mode coupler that is defined by the dimensions of the grating. Couplers based on the Bragg grating are wavelength-specific and cannot be used for the coupling from the broadband source. To couple polychromatic light, the edge coupler one can use the [36, 56]. For edge couplers, the waveguide dimensions experience deformation along the propagation direction dictated by vector **k**, as shown in Figure 2k. This method solves the modal mismatch. Fiber-lenses can also be used to efficiently focus the source into the waveguide facet.

2.2 Active components

As aforementioned, one of the major issues in on-chip nanophotonics is the coupling of light to the waveguide. To overcome this problem, the source can be directly fabricated on a chip. The coupling efficiency can be improved by fabricating the laser on a chip, and a low pump pulse energy can be used. In order to make a tunable narrowband laser on a chip, a ring resonator made of Si wire was used [43, 44]. We note that for the broadband sources, silicon cannot be used, as its small band-gap limits infrared emission [57]. Silicon nitride, however, can be used for broadband generation using supercontinuum generation from visible to mid-infrared [57] such as supercontinuum generation, as shown in Figure 3a, b, or octave-spanning supercontinuum generation [61], and pulsed lasers on a chip for efficient and local means for light control [62, 63].

Another important requirement of on-chip photonics is *optical modulation*. Modulation is a change in one or more properties of light such as frequency, amplitude or phase by changing the refractive index of the medium. The main method to change the refractive index is by applying field on the material, creating an electro-optic effect [64]. This effect is divided into two types; *electro-refraction* – a change in the real part of complex refractive index and *electro-absorption* – a change in the imaginary part of complex refractive index. However, silicon, which is common material for on-chip photonic devices, has a weak electro-optic effect. Therefore, the more efficient effect of modulation is by the plasma dispersion. This effect is weak for electro-absorption modulation but can be used for phase modulation that in turn can be changed to modulate the intensity using Mach–Zehnder interferometers or ring resonators. This improves the change in order of magnitude. Few waveguide-based configurations can be used for modulation. A Mach–Zehnder can be used as an amplitude modulator by creating phase shift in one of its arms (Figure 3c) [58, 65] and a ring-resonator which has a compact footprint and a low drive-voltages [46, 66].

To detect an optical signal on a chip, *detectors* also can be monolithically integrated on the same planar platform. For this, the Schottky diode structure is widely used. Such diode is made of metal layer placed on a doped semiconductor, creates a Schottky barrier. Detection occurs when the carrier created by the absorption has enough energy to pass this barrier. To implement the detection concept on a chip, one can place a metal film on doped silicon, which creates a Schottky diode-based detector [59]. Using a gold strip as a metal layer, a low Schottky barrier can be produced, which in turn improves the quantum efficiency of the device [67]. Another material widely used in on-chip detectors is germanium. Germanium can achieve a higher absorption coefficient in the near-infrared compared to silicon. Evanescently-coupled germanium waveguide photodetectors on an SOI platform can be used for photodetectors at the telecommunication windows [60].

In recent years, graphene plays an important role in tuning active devices in on-chip photonics to achieve novel capabilities [69]. Graphene is a two-dimensional layer of carbon in a hexagonal configuration which has high carrier mobility [70, 71] and broadband absorption [72]. These properties allow for the design of fast devices [73]. One of the prominent utilization of graphene is the modulation of light. By placing a layer of graphene on silicon-on-insulator (SOI) waveguide (Figure 4a, b) and applying the bias, one can change the properties of the graphene to modulate the amplitude [68, 74]. In addition, by placing graphene on a silicon nitride ring resonator (Figure 4c, d), one can tune the spectral location of the resonance [45, 47].

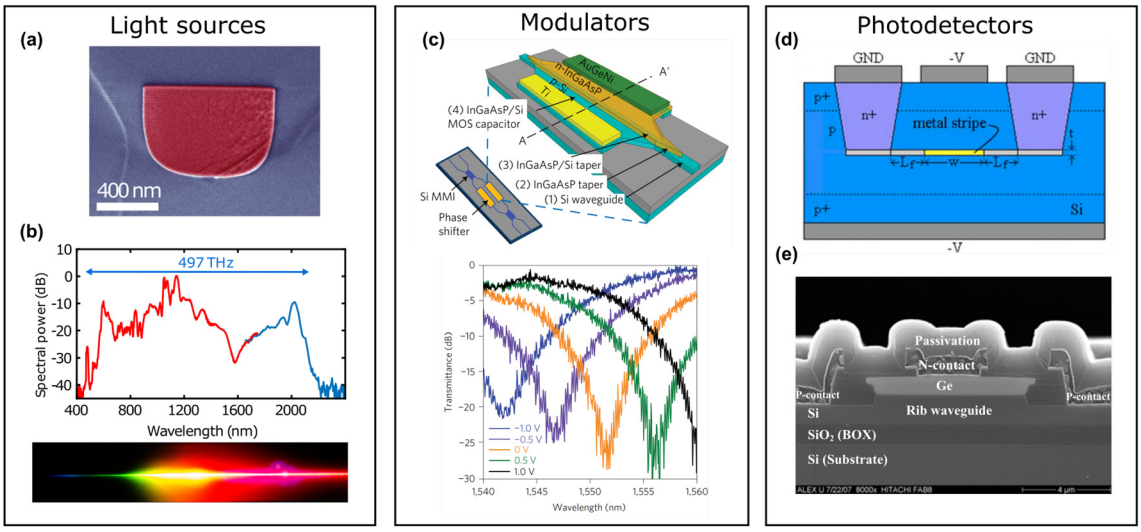

Figure 3: Key active components in on-chip nanophotonics. (a) SEM image (false color) of a waveguide facet and (b) Supercontinuum spectrum generated in a 5.5 mm long Si_3N_4 waveguide with $h = 1$ µm, $w = 0.8$ µm, and $E_p = 590$ pJ with photograph of the spectrum after being dispersed by a diffraction grating (reproduced from [57]). (c) Schematic of the InGaAsP/Si MOS capacitor MZ modulator (top) and Measured spectrum of an MZ modulator with 700-µm-long phase shifter as a function of applied voltage (bottom) (reproduced from [58]). (d) Surface-plasmon Schottky contact detector based on a metal stripe buried in silicon (reproduced from [59]). (e) Cross-section SEM image of Ge waveguide photodetector (reproduced from [60]).

Graphene can be also used as a laser source on a chip, allowing for the widest wavelength-tuning in Vertical-external-cavity surface-emitting-lasers (VECSELs) [75].

3 Guided-wave devices for emerging applications

Recently, guided wave devices on a chip find a use for emerging applications such as overtone spectroscopy. The ability to probe the molecular fundamental vibrations or overtones (high harmonics) vibrations is fundamental to modern healthcare monitoring techniques and sensing technologies since it provides information about the molecular structure and dynamics. However, the absorption cross-section of molecular vibration overtones is much smaller compared to the absorption cross-section of fundamental vibrations, and therefore their detection is challenging. Nevertheless, recent works on waveguides and microfibers show that molecular overtones can be

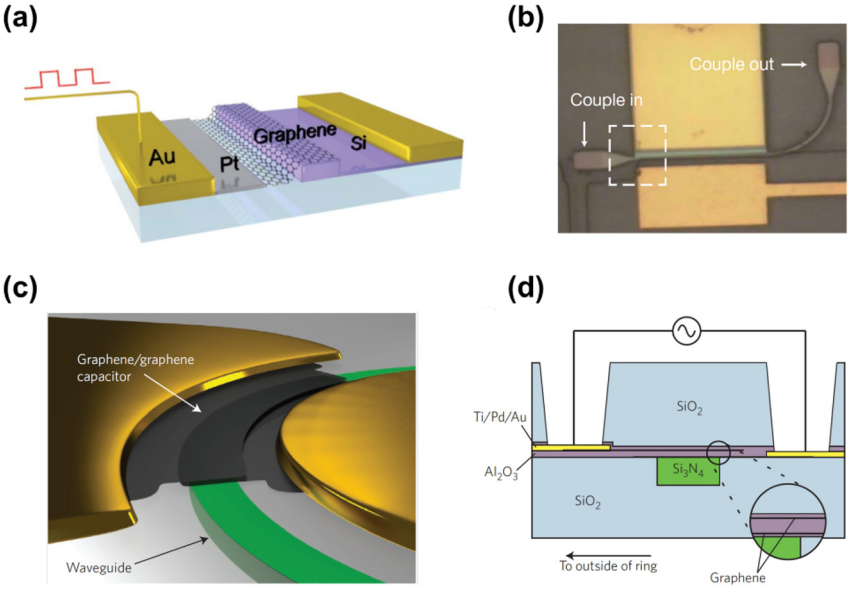

Figure 4: Graphene based devices. (a) A graphene-based waveguide-integrated optical modulator. (b) Top-view optical microscope image of the waveguide ((a) and (b) are reproduced from [68]). (c) Schematic of the modulator consisting of a graphene/graphene capacitor integrated along a ring resonator. (d) Cross-section of the device. Two layers of graphene separated by 65 nm interlayer Al_2O_3 dielectric form a parallel-plate capacitor. ((c) and (d) are reproduced from [45]).

probed with on-chip nanophotonic devices [1, 41, 76–80] which we overview in the section below.

3.1 Overtone spectroscopy on a chip

Spectroscopy focuses on the interaction between the radiation and matter [81] and can be used for remote and on-site detection. The matter–radiation interaction changes the energy of the molecule, resulting in absorption or emission bands in the transmission spectrum. A molecule can have five types of energy: translational, rotational, vibrational, electronic, and spin. Those energies occur in different regions of the electromagnetic spectrum. For example, when illuminated with infrared (IR) radiation, the atoms in the molecule start to vibrate. Each atomic bond vibrates in different modes, resulting in different absorption bands for different atomic bonds that give information about the molecular structure.

IR spectroscopy, also named vibration spectroscopy, is an important analytical technique because it can provide information on a molecule in different states of matter: liquid, solid, or gas. IR spectroscopy can be mainly divided into two spectral regions: mid-infrared (mid-IR) and near-infrared (near-IR). The mid-IR ranges from 2.5 to 25 μm and the near-IR ranges from 0.8 to 2.5 μm [82]. In the mid-IR, the fundamental vibration can be excited, resulting in well-defined absorption lines. The overtone (high harmonic) vibrations are excited in the near-IR due to the higher energy that is needed to cause the overtone transitions. Detection in each spectral range has its drawbacks and advantages. For example, near-IR can be used for applications with water as a solvent due to low absorption of H_2O molecules in near-IR, whereas mid-IR can be used for organic functional groups due to the well-defined absorption bands in mid-IR.

There are two methods for light–matter spectroscopy in the infrared region: direct interaction (plane wave) and evanescent field interaction.

The most common method for spectroscopy is a direct interaction between the radiation and the analyte. The plane wave interacts with the sample and the transmitted light is collected by the detector. Conventional infrared spectrometers are based on the direct interaction and use Michelson interferometer for changing the wavelength range of the incident beam. These spectrometers use a Fourier transform (FT) technique. FT algorithm is needed for converting the output power, which is a function of mirror displacement to a function of wavelengths. An FTIR spectrometer exhibits high resolution and can be used for a variety of applications. However, a Fourier transform-based spectrometer is too large for a chip-scale sensor and cannot be used for real-time monitoring. Furthermore, an FTIR spectrometer collects the entire signal and then converts it to power as a function of wavelength. As a result, when a noise occurs in some regions, it added to the entire spectrum. Therefore, for an FTIR spectrometer, noise in a certain region affects the entire spectrum.

To overcome these drawbacks, optical dispersion can be used instead of the Fourier transform-based technique. In a dispersive spectrometer, the spectrum is separated optically, using components such as a prism and a slit, and not by analytical calculations. As a result, a dispersive spectrometer does not affect the spectrum with unnecessary noise.

Optical guided wave structures, on the other hand, can be used for remote and on-site chip-scale detection [1]. They allow for chip-scale dimensions and require no adjustments of optical or mechanical components as required in the FTIR spectrometer [83]. Guided-wave optical structures are made of a substrate, guiding layer, and superstrate. As we mentioned above, the light propagates in the guiding layer n_2 due to total internal reflection. The guiding layer needs to have a higher refractive index than the surrounding n_2 to allow the waveguide condition, $n_2 > n_1$, for instance as in on-chip direct interaction sensor [84]. A nanofluidic slot waveguide was utilized for mid-IR spectroscopy. In a slot waveguide, the electromagnetic field is guided by the lower index guiding layer [85]. Therefore, it allows using the analyte as the guiding layer. The slot waveguide scheme enhances the sensitivity and allows to detect common chemicals such as isopropanol.

Another spectroscopic method is based on the evanescent field detection. Along the propagation, in a guided wave structure, a fraction of the field can penetrate beyond the guiding layer and exponentially decays in the direction perpendicular to the propagation direction – $\vec{k}$, which is called the evanescent field. Guided wave structures can be used for an evanescent field sensor, which is also named attenuated total reflection (ATR) sensor. The sensing mechanism is based on the interaction between the evanescent field and the analyte. A big advantage of ATR spectroscopy is that it requires little or no sample preparation. In addition, ATR is good for highly absorptive samples [86] due to the small penetration depth of the evanescent field.

Ring-resonator architecture, which is an example of an evanescent field sensor [32], shows enhanced sensitivity due to the heavy influence of the resonator environment. It can sense temperature, refractive index, and even strain. The resolution of the sensor is defined by the

wavelength distance between two resonances (FSR – free spectral range). Previous work [48] demonstrated the ability to identify the spectra of *N*-methylaniline (NMA) from 1.46 to 1.6 μm with a resolution of 1 nm using a microring resonator. However, it cannot provide broadband sensing [48] due to limitations of the FSR-based method.

There is another group of sensors named refractometers (Figure 6a from [3]). Refractometers are sensors that detect changes in the refractive index of the analyte as shown in Figure 6c [3, 87, 88]. Refractometers can achieve high sensitivity for a refractive index change with a resolution of 5.4×10^{-5} [87]. However, refractometers lack specificity, namely the ability to identify analytes or biological samples with similar (or the same) refractive index.

In 2016, optical glass waveguides were shown their use for the first time, for the detection of overtone transitions in near-infrared. In their experimental work, authors [76] reported on the giant enhancement of the absorption of light in solutions of organic molecules due to the switch from ballistic to diffusive propagation of light through a channel silicate glass waveguide. The authors observed enhancement in diffusion regime as high as factor 300 in *N*-methylaniline and by a factor of 80 in Aniline compared to the expected values in the case of ballistic propagation of light in a waveguide. Figure 5a shows a photograph of the waveguide with a polydimethylsiloxane (PDMS) liquid

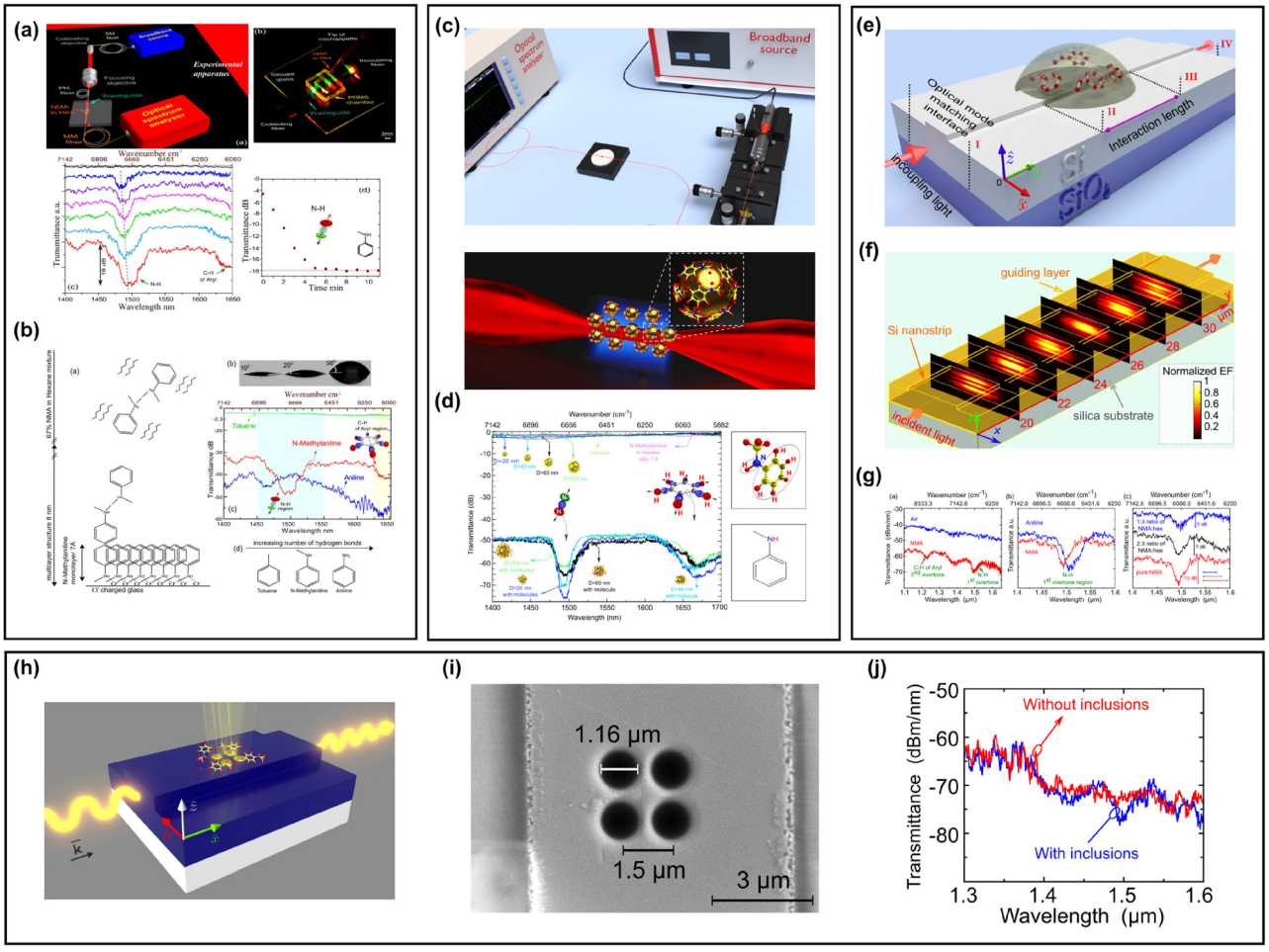

Figure 5: Overtone spectroscopy using guided wave structures. (a) Experimental apparatus and recorded spectra of NMA molecules adsorbed on the waveguide. (b) Responses from benzene molecules with different substituents demonstrating the influence of hydrogen bonding ((a) and (b) are reproduced from [76]). (c) Experimental apparatus (top) and sculptured microfiber architecture (bottom) and (d) the experimental results on the microfiber and the chemical structure of NMA (reproduced from [77]). (e) Schematic of Si nanostrip rib on-chip sensor, (f) evolution of the interfered guided modes in the interaction length with the analyte and (g) Measured spectrum from Si nanostrip rib waveguide embedded in NMA molecules, aniline and different mixture ratios of *N*-methylaniline in hexane (reproduced from [78]). (h) Schematic of the dielectric rib waveguide with cluster of inclusions of cylindrical shape, (i) SEM image of the fabricated inclusions on the rib waveguide and (j) Measured transmittance spectra with on reference waveguide (red curve) and on waveguide with inclusions (blue curve) ((h)–(j) are reproduced from [41]).

reservoir with input/output fibers guiding green and red laser lights for demonstration of potential multi-array detection. Figure 5a shows the time evolution of the relevant transmittance spectra. The effective concentration of NMA in the vicinity of the waveguide surface increases with time and eventually achieves the maximum loss of about –18 dB (Figure 5a) which corresponds to the loss measured for the pure NMA sample in a cuvette. The polar N–H bond in NMA can align with the polar surface, and the non-polar benzene ring aligns with the solvent, relieving the surface tension (Figure 5b [left]). Contact angle measurements are shown in Figure 5b (right) confirm the waveguide surface modification due to adsorption.

Following this discovery, later in 2018, Karabchevsky et al. reported on an unexpected enhancement of the absorption of near-infrared light by aromatic amine overtones on photonic microfibers sculptured with gold nanoparticles [77]. The experimental setup for this work and a schematic representation of the microfiber sculptured with gold nanoparticles are shown in Figure 5c. On a bare microfiber that had not been sculptured by gold nanoparticles there was no molecular signatures observed (upper spectrum in Figure 5d) in contrast to the spectra obtained on the microfibers sculptured with gold nanoparticles (lower part of Figure 5d). In addition, waveguides in microfiber configuration were used to monitor the cancer treatment efficiency in real-time [79].

In the same year, Katiyi and Karabchevsky reported on a new chip-scale nanophotonic device that utilizes near-IR absorption by molecular overtones vibrations for label-free chemical sensing on silicon waveguides [78]. The authors designed a multimode silicon nanostrip waveguide in such a way that launching the high-order modes improves the sensitivity of the chip-scale device for broadband detection. Such a sensor is shown in Figure 5e and has dimensions of 5 mm (L) × 5 mm (W) × 1 mm (D) and supports

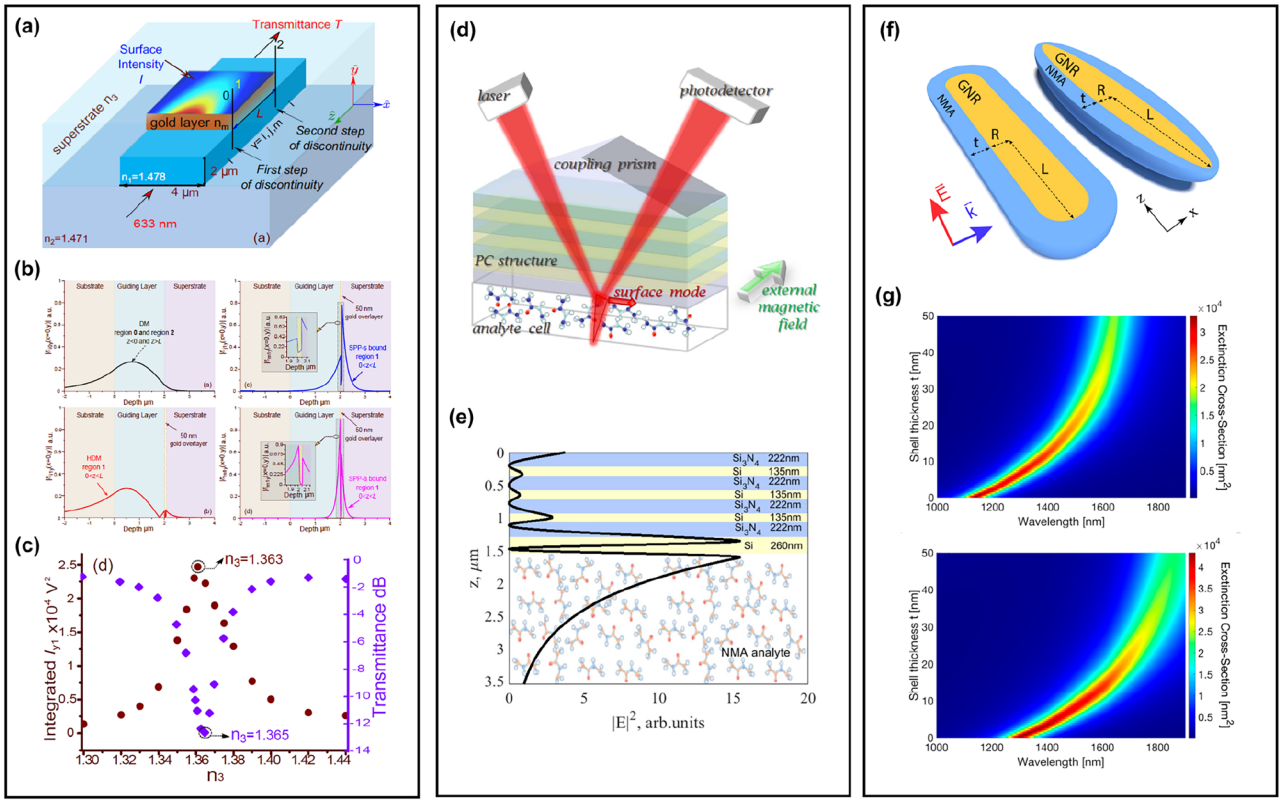

Figure 6: Surface plasmon-based waveguide sensors. (a) 3D schematic of composite plasmonic waveguide. (b) Cross-sections of the y-component of the electric field magnitude for the structure: a purely dielectric mode (DM) in a dielectric waveguide and in a gold coated region for hybrid dielectric mode (HDM), SPP-s and SPP-a. (c) The superstrate indices, n_3 which yield the minimum in transmittance and the maximum in integrated surface intensity ((a)–(c) are reproduced from [3]). (d) Schematic representation of the multilayered stack of the photonic crystal (PC) nanostructure sensor. (e) PC structure scheme and the electromagnetic field distribution of the mode inside the PC structure and NMA analyte ((d) and (e) are reproduced from [89]). (f) Schematics of systems with gold nanorods (left) studied in numerical simulations and nanoellipsoids (right) used in the analytical model. (g) Extinction cross-sections of gold nanoellipsoids with NMA shells of different thicknesses (top). The semi-major axis of the gold core is $L = 55.9$ nm (bottom). The semi-major axis of the gold core is $L = 68.1$ nm ((f) and (g) are reproduced from [80]).

nine guided modes. Due to the large evanescent field and increased interaction with the analyte, high order modes contribute to the sensitivity of the sensor. It demonstrates the ability to detect and study the absorption of different mixtures ratio of NMA:Hexane using a silicon rib waveguide and differences in the transmission of *N*-methylaniline and Aniline as shown in Figure 5g. Next, the authors investigated the influence of an inclusion cluster on Talbot effect [41]. For this, an on-chip multimode silicon nanostrip waveguide with an inclusion cluster was fabricated and tested (see Figure 5h). The inclusion of cylindrical shape with the diameter comparable to the wavelength is shown in Figure 5i. It was found that due to the scattered field caused by the deflected Talbot effect, the absorption line of N–H bond of *N*-methylaniline around 1.5 μm was identified (see Figure 5j).

Waveguides are also widely used as on-chip sensors refractometers. The detailed analysis of the excitation and propagation of modes in channel photonic waveguides overlaid with a short section of plasmonic overlayer made of gold was reported in Ref. [3] (the configuration is shown in Figure 6a). These have then been used to illustrate the behavior of the complex expansion coefficients into and out of the metal coated region, which are discussed in terms of power conservation. Using this approach, the transmittance of such a channel waveguide SPR refractometer is calculated as a function of the refractive index of the superstrate. Figure 6b shows cross-sections of the dominant y-component of the electric field magnitude supported by the dielectric waveguide and composite plasmonic waveguide. The surface intensity integrated across the full width of the waveguide and along the length from $z = 0$ to $z = 200$ mm for varying superstrate index is shown in Figure 6c, yielding the highest integrated surface intensity at $n_3 = 1.363$ which corresponds to the highest excitation (expansion coefficient) of the hybrid dielectric mode. This theoretical study enables clear understanding of the complex behavior of modes in composite dielectric-plasmonic waveguides and design of optimized sensitive miniature devices for refractometry, evanescent vibrational spectroscopy and plasmonic devices for all-optical processing, harnessing the advantages of both dielectric and plasmonic waveguides. The model developed is general and can be used to design and optimize composite waveguides with more complex overlayer structures. Additional waveguide designs have been implemented [90] with the goal of increasing the surface plasmon polariton distance, including the use of nanojets [91].

Recently, Borovkova et al. proposed high-Q magnetophotonic structures for a supersensitive detection of weak absorption resonances in the near-IR [89]. The utilization of all-dielectric magnetophotonic structures for sensing of the imaginary part of the permittivity having very weak resonances in the near-IR was investigated. The authors analyzed the contributions of both magnetic and nonmagnetic photonic crystal (PC) configurations for the detection of weak molecular transitions overtones. The designed PC structures are shown in Figure 6d which supports the excitation of the long-range propagating quasi-surface electromagnetic modes. The excited mode represents a guiding mode localized in the terminating layer of the PC structure due to the PC bandgap (BG) on the one side and total internal reflection on the other. In order to excite the quasi-surface electromagnetic mode at the PC–analyte interface, the authors designed the PC-based structure, shown in Figure 6e. By exciting the quasi-surface modes, well known for their extreme sensitivity to the materials' properties, the weak absorption peaks corresponding to the higher harmonics (molecular overtones) of the N–H vibrational transitions can be efficiently detected.

The mechanism of local field enhancement in molecular overtones was explored for the first time by Dadadzhanov et al. [80]. Authors theoretically explore yet unclear possibilities to enhance absorption by molecular overtone transitions in the near-field of plasmonic nanoantennas such as gold nanorods (GNRs) due to the combination of localized surface plasmon resonance (LSPR) and lightning rod effect. The contribution of gold nanorods parameters, shown in Figure 6f, on the effect of surface-enhanced near-IR absorption (SENIRA) by molecular overtones. It is interesting to note, that the differential extinction provides the SENIRA with two orders of magnitude enhancement.

4 On-chip quantum nanophotonics

In order to explore quantum phenomenon, there is a need to generate, manipulate, and detect a single photon. Photons are an excellent low-noise carrier of quantum information, due to their weak coupling with the environment, leading to their immunity from the decoherence issues of matter-based systems. Investigations of quantum science led to results such as tests of entanglement, generation of squeezed light, and demonstrations of quantum teleportation [92]. Bringing this to the real world would be advantageous for tasks in communication, computation, and simulation. However, highly complex manufacturing of quantum technology, with large component counts is a challenge. Given the combination of single photons is quantum information carriers and chip-scale fabrication techniques. On-chip quantum photonics is an attractive platform for quantum technologies.

4.1 Material platforms and devices in on-chip quantum photonics

With the first on-chip photonic quantum logic gate demonstrated in 2008 [93], on-chip quantum photonics is still relatively new. In spite of its immaturity, on-chip quantum photonics uses common tools from the CMOS industry. Quantum information processing using hundreds or thousands of photons will require technologies and scaling functionalities that can only be provided by the on-chip photonics. A range of on-chip photonic platforms have been developed, including single-photon sources (SPSs), linear-optic quantum circuits, and integrated single-photon detectors (SPDs), with applications toward the chip-scale quantum communications, quantum computing and information processing, Boson sampling, and quantum simulation of chemical and physical systems.

4.1.1 Single photon sources

On-chip generation of a large number of identical single photons is required in order to use the full capabilities of on-chip quantum photonics. Using the spontaneous four-wave mixing or the spontaneous parametric down-conversion process, photon pairs can be generated from nonlinear waveguides. Single photon sources have been demonstrated in waveguides composed of χ^3 materials [98–100] and χ^2 materials [101, 102]. A feature of on-chip parametric sources is that they can be made into highly identical arrays without sacrificing controllability; however, photon production is non-deterministic, which can be improved by using multiplexing. For deterministic single photon generation, quantum dots in PC waveguides allow preferential emission into the waveguide [103]. Creating multiple single photon sources from quantum dots is a challenge due to the difficulty in uniformity between the dots, and inhomogeneous broadening. However, embedding quantum dots into nanowires [94], as can be seen in Figure 7a, has shown a source efficiency of 0.72. Actively de-multiplexing the single photons into different spatial modes is a solution [104], which produces multiple photons at a reduced rate. Single-photon source based on a single neutral nitrogen-vacancy center in a diamond diode structure [95] was reported and is shown in Figure 7b.

4.1.2 Single photon detectors

To read out the quantum information, on-chip detection of single photons is also required. Technologies such as avalanche photodiodes, superconducting nanowire single-photon detectors, and transition edge sensors are used for single photon-detection. Transition-edge sensors utilize the evanescent field of the waveguide's guided mode and

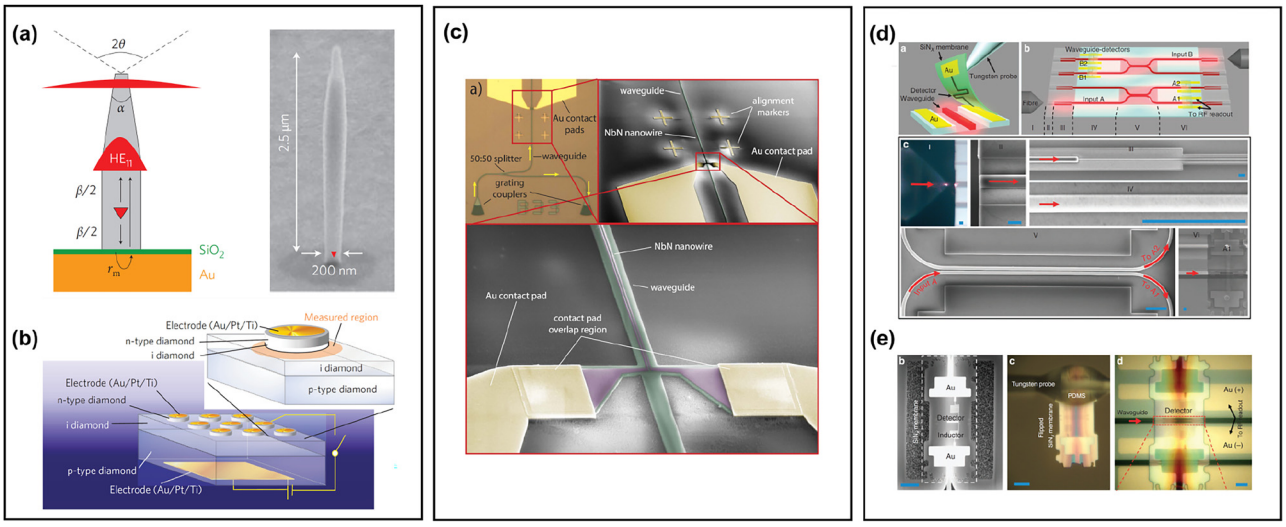

Figure 7: On-chip quantum photonics. (a) Single-photon source geometry. An InAs QD (red triangle) is embedded in a GaAs photonic nanowire and SEM image of a typical device (reproduced from [94]). (b) Schematic diagram of the single-photon-emitting diode of diamond (reproduced from [95]). (c) Optical microscope image of a nanophotonic circuit with on-chip SNSPD device. Inset: SEM micrograph of the detector area with metal alignment mark and zoomed waveguide region with NbN nanowire atop (reproduced from [96]). (d) Assembly of high-system-efficiency PIC with on-chip detectors via membrane transfer. (e) (left) SEM of suspended SiN_x membrane with detector on top (middle). The detector was removed from the carrier chip using a tungsten microprobe containing a drop of hardened PDMS near the tip (right). Optical micrograph of an SNSPD integrated with a silicon waveguide ((d) and (e) are reproduced from [97]).

potentially allows extended interaction regions [105], but they are plagued by very slow response times and require cooling [106]. Detectors based on superconducting nanowires, such as the one shown in Figure 7c–e, similarly operate at cryogenic temperatures only. Recent waveguide-coupled Ge-on-Si avalanche photodiodes showed that single photon detection in room temperature conditions was possible [107]; a similar Ge-on-Si photodiode with a different design showed a detection efficiency of 38% at 125 K [108].

4.2 Applications of quantum chip-scale devices

Communication is one of the important applications in everyday life, consequently, the search for important and sensitive information protection never ends. However, the communication is whereas cryptography provides numerous methods to ensure that communications are secure against eavesdropping attacks and impersonating a hostile factor and exposing encrypted content. By sharing encrypted keys between the transmitter and receiver based on the law of quantum mechanics, one can achieve security which is inaccessible by classical communications.

4.2.1 Quantum cryptography

The common, well-known and developed application of quantum cryptography is the quantum key distribution (QKD), which describes the use of quantum mechanical effects to perform cryptographic tasks or to break cryptographic systems. Utilizing the advantages of on-chip photonics allows the ability to realize QKD transmitters and receivers which is a more robust, miniaturized and low-cost platform.

4.3 Computing with cold atoms and waveguides

On-chip nanophotonics plays a major role also in information distribution, while the degree of optical functionality integrated in information processing systems remains extremely limited, and they have yet to fully benefit from fundamental and technological achievements in recent decades. Control of light-cold atoms interaction on waveguides and all-optical logics with waveguides are building blocks toward realization of information processing on optical chip. The combination of both creates a type of on-chip device with the best of both worlds: on one hand, the long coherence times of isolated cold atoms and on the other hand accuracy, density, miniaturization and integration of optical logic elements. In addition, control of light-cold atoms interactions on optical chip are at the forefront of quantum physics, and pose challenges to our understanding of quantum phenomena such as: quantum interference [109] probing of Johnson (thermally-induced) noise [110–112], electron transport [113], the testing of the Casimir–Polder potential near surfaces [111, 114, 115], quantum reflection from surfaces [116], investigations of degenerate Bose gases in low dimensions [117–119], statistical many-body features such as thermalization [120–122], entanglement [123–125] and squeezing [126] effects in an interacting Bose gas, to list a few; and for technological advances in, quantum metrology, entanglement, non-destructive detection, quantum communications [127] and more. Photonic waveguide architecture allows unprecedented control of photons in the quantum regime.

To date, the experimental platforms in which waveguides has been demonstrated mainly include ultracold atoms, trapped ions and photonic networks. Ultracold atoms and ions have so far achieved the most success in this field, including measurement of the dynamics and equation-of-state for Bose and Fermi gases, with controlled interaction strengths and reduced dimensions, studies of Bose and Fermi Hubbard models of atoms loaded into optical lattices such as the Mott-insulator transition [128] and the ‘Higgs’ amplitude mode [129]. In addition, the implementation of artificial magnetic fields through the coupling of internal and external degrees of freedom of the atoms with Raman beams to simulate spin–orbit coupling [130] and the spin-Hall effect in atomic gases [131] was presented. Complex waveguide based devices fabricated in material systems such as InP, GaAs, silicon, and silica have been used to develop commercial components for transmitting, routing, and detecting high-speed optical signals for data communication systems. Waveguides platform have also been employed in single-photon quantum key distribution (QKD) systems for use as time-bin entanglement circuits [132, 133]. Despite demonstrations such as quantum interference on a waveguide [109], it is essential that high visibility non-classical interference can be routinely achieved in waveguide circuits for on-chip quantum photonics to be a viable. This was first demonstrated by Politi et al. [93]. Despite the many promising advantages, the integration of optical waveguides structures for atom trapping, on a robust platform, together with additional elements for atomic state manipulation and detection remains a great challenge.

4.4 $\mathcal{PT}$-symmetric waveguides

A number of intriguing properties in photonics are related to the non-Hermitian Hamiltonians possessing parity-time ($\mathcal{PT}$) symmetry that is the symmetry with respect to the simultaneous coordinate and time reversal [134]. Recently, it has been also studied in guided-wave optics. A possibility of the experimental investigation of the $\mathcal{PT}$-symmetric structures certainly heats up the interest to this subject in optics [135–138] in order to apply these systems for sensing [139, 140], lasing, and coherent perfect absorption (anti-lasing) [141, 142].

It was Purcell who revealed that a spontaneous emission rate is not an intrinsic property of the emitter, but is proportional to the local density of modes (density of photonic states) in the vicinity of the transition frequency [143]. In other words, the spontaneous emission rate is determined by an environment. Phenomenon of the spontaneous emission enhancement owing to the influence of the environment is known now as the Purcell effect. The enhancement is defined as a ratio of the spontaneous emission rate in the system under consideration to that in the free space [144]. With the development of nanotechnology, nanophotonics opens up new avenues for engineering spontaneous emission of quantum emitters in specific surrounding media [145–150] including non-Hermitian media. Investigation of the spontaneous emission of the dipole emitter inside a $\mathcal{PT}$-symmetric planar cavity has been recently performed by Akbarzadeh et al. in Ref. [151]. The authors have found suppression of the spontaneous relaxation rate of a two-level atom below the vacuum level. A general theory of the spontaneous emission at the exceptional points of non-Hermitian systems was developed in Ref. [152] and revealed finite enhancement factors.

A number of methods including numerical techniques [153] have been developed for calculation of the Purcell factor of dipole and quadrupole emitters in various environments. The most general one is based on calculation of Green's dyadics $\widehat{G}(r, r_0)$. Since the photonic local density of states is proportional to the imaginary part of the dyadic $\mathrm{Im}\widehat{G}(r_0, r_0)$ [154], the purely quantum phenomenon of spontaneous emission can be reduced to the problem of classical electrodynamics. The Purcell factor $F_p = P/P_0$ can be written in terms of the powers P and P_0 emitted by a source in an environment and in the free space, respectively. This approach is widely adopted and can be exploited, e.g., for description of the spontaneous relaxation of molecules in absorbing planar cavities [155], explanation of the surface-enhanced Raman scattering [156], finding anomalous Purcell factor scaling in hyperbolic metamaterials [157], etc.

The Purcell factor can be calculated separately for each of the discrete scattering channels. Due to the highly demanding field of photonic integrated circuitry (PIC) offering chip-scale miniaturization of actual devices and transformation of academy governed knowledge to the industry, recently the research has been accelerated toward utilization of important optical phenomena in on-chip photonic devices. For instance, just a couple of years ago, the modal Purcell factor for the basic element of PIC planar waveguide was introduced within the scattering matrix formalism [158]. A year after, another approach based on application of the reciprocity theorem was developed and successfully exploited in a ring resonator configuration [159].

5 Manipulation of light on a chip with metasurfaces

Metasurfaces (man-made surfaces) control the electromagnetic fields and can achieve functionalities not available with natural materials. Metasurfaces allow controlling the phase, the amplitude and the polarization by subwavelength dimensions. They made of subwavelength structures such as nanorods and nanoholes (scatterers). For instance, by creating negative relative permittivity and permeability values, effect of negative refraction occurs. Metamaterials can be used for phase compensation medium when combining double negative media and positive indexed materials are combined. A negative refractive index equal to –1 allows creating superlens which breaks the limitation of a square of wavelength focusing by guided-wave optics [160]. In addition, metasurfaces allow creating near-zero refractive index in which one or more parameters, such as relative permittivity or relative permeability, are near-zero [22] and to enhancing the nonlinear refractive index [161].

One of the interesting implementations of metamaterials is an invisibility cloaking effect. Galutin et al. showed that the invisibility cloaking effect can be demonstrated with waveguides when the metasurface overlayer affects the scattering fields of an object located on the cloak so they do not interact with the evanescent field, resulting in an object's invisibility [6]. The modal distribution and surface intensity in a channel photonic waveguide with a cloaking metasurface overlayer was studied for which the composite plasmonic

waveguide structure is shown in Figure 8a. The plasmonic metasurface is placed on the composite plasmonic waveguide with the nano-spacer. High dielectric nano-spacer made of Si has contributed to the light confinement in the vicinity with the metasurface boundary and facilitated the coupling to the hybrid plasmonic modes. The light manipulation is realized due to the engineered effective permittivity which in turn avoids the scattering effect. Figure 8b shows the transformed grids and refractive index of the evanescent field waveguide cloak. Figure 8c shows the surface intensities of waveguide evanescent field cloak on a chip with (up). Reference waveguide and (down) with-cloak and the cylindrical object.

Metasurfaces engraved on a waveguide can be utilized to exhibit mode conversion effects. Mode conversion can be realized with dielectric metasurfaces engraved in the silicon waveguide as reported by Greenberg and Karabchevsky [25]. In order to efficiently couple between the *m*th and *n*th modes in a waveguide, an effective wavevector k_{eff} must be provided by the metasurface to overcome the propagation constant mismatch. The proposed by authors SOI waveguide strip waveguide with a periodic index perturbation along the propagation direction is shown in Figure 8d. Figure 8e shows calculated results of TE_0–TE_1 (E_y component) mode conversion device: input and output mode profiles, refractive index profile required for conversion, and mode evolution along the propagation direction. The conversion efficiencies of 95.4% between the TE_0–TE_1 modes over 8.91 μm interaction distance and 96.4% between the TE_0–TE_2 over 6.32 μm were obtained. The resulting coupling coefficient changes as a function of the interaction distance in a sinusoidal manner, which is crucial for constructive energy transfer from one mode to another.

5.1 On-chip optical vortex

An ever-growing demand for compact integration gives rise to integrated photonic devices on different material platforms for emerging applications among them an on-chip biosensors, on-chip quantum technologies and recently even the on-chip optical vortex based detectors in plasmonic materials [162].

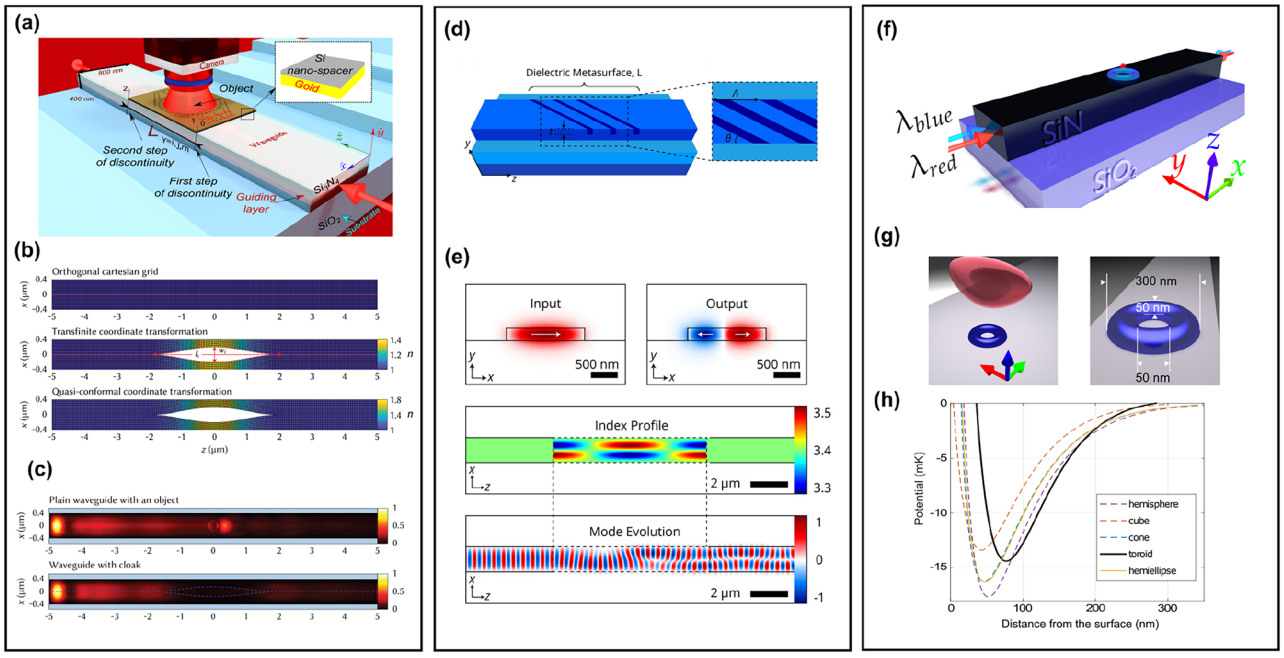

Figure 8: On-chip nanophotonic devices for emerging applications: (a) Schematics of the composite plasmonic waveguide structure and materials to study the invisibility cloaking scheme. (b) Transformed grids and refractive index of the evanescent field waveguide cloak. (c) Surface intensities of waveguide evanescent field cloak on a chip with (up) Reference waveguide with cylindrical object placed on top and (down) with cloak a cylindrical object. ((a) and (c) are reproduced from [6]). (d) Schematic configuration of the proposed mode converter composed from the profiled refractive index as tilted periodic slits. (e) Calculated results of TE_0–TE_1 (E_y component) mode conversion device: input and output mode profiles, refractive index profile required for conversion, and mode evolution along the propagation direction. ((d) and (e) are reproduced from [25]). (f) Illustration of the ridge waveguide, bi-chromatic incident light, and the silicon nano-antenna (not to scale). (g) Potential isosurface at the zero-point energy for the toroid nano-antenna and the nano-antenna shape and dimensions (all units in nm). (h) Potential dependence on *z* where $x = y = 0$ ((f)–(h) are reproduced from [37]).

An optical vortex is a beam of light that propagates in a way that the phase experiences phenomenological singularity and the wavefront has a topological structure with topological charge due to the helicoidal spatial wavefront around this phase singularity. Such a topological structure can be found in many disciplines among them in optics acoustics, and others. To understand the influence of the singularity, one has to explore the phase, polarization, and amplitude of the incident beam. While exploring these properties of the special beam, one may discover that both the polarization and the amplitude vanish and the phase cannot be determined. These insights were published as a new concept in wave theory back in 1974. In their theoretical work, Nye and Berry reported on observation of so-called dislocations [163].

First on-chip silicon-integrated optical vortex emitter was reported in *Science* [164]. Having *emitter* and *detector* monolithically integrated on the same chip would be an essential step in on-chip optical vortex-based photonic devices. In their experimental work, Feng and coworkers developed a novel on-chip optical detector which allows to fully characterize the polarization and phase singularity based on plasmonic Spin-Hall nano-grating. Their method of detection is different from other state-of-the-art systems because it allows for the detection of singularities simultaneously. Interestingly, the detector developed by Feng and coworkers does not require complicated alignment. It is based on an asymmetric metallic array, in which the top and bottom part of the array has different grating constant. The specific surface topology dictates an angle in which excited surface plasmon polariton (SPP) will propagate. The asymmetry allows differentiating the sign of the topological charge (phase) while the Spin-Hall slits are sensitive to the spin of the incoming beam. The so-called Spin-Hall slits are composed of nanoslits oriented at $\pi/2$. Such orientation of the nanoslits gives rise to the chiral response of the detector. If the slits are reversed, the inverted chiral response takes place. This special design allows the authors to distinguish between the left-circularly polarized (LCP) beam or right-circularly polarized (RCP) beam. Simply put, a beam incident on the detector would excite an SPP which travels at an angle θ to one of the four quadrants, see Figure 1 in ref. [162]. The quadrant in which the SPP propagates determines the polarization (RCP/LCP) of the beam and the sign of the topological charge. The angle θ dictates the magnitude of the topological charge. The great advantage of such devices is their ultra-compact size and extremely simple operation [164, 165], which make them easy to integrate with other on-chip components, such as modulators and lasers, to form photonic integrated circuits, enabling large-scale integrated photonic applications.

The next milestone to achieve in on-chip optical vortex-based devices would be to demonstrate the operation by eliminating inevitable Ohmic losses of plasmonic materials and exploring other surface waves such as Bloch waves which in turn can propagate on lossless dielectric materials [1, 23, 37, 166–169]. One can expect significant advances in integrated photonics in the coming years in the direction of optical vortex-based on-chip novel devices.

6 Global trends and future challenges

A key advantage of on-chip nanophotonics is its ability to facilitate the miniaturization while studying the interaction of light with matter on a chip but at the scale where optical, electronic, structural, thermal and mechanical properties are deeply interdependent. The far-reaching goal of on-chip nanophotonics is to control light fast within only a few oscillation cycles of the light wave, in a miniature device containing only a few layers of atoms using signals carried by only a few photons for emerging applications ranging from quantum technology to biosensors of dangerous viruses with ultra-high sensitivity. By translating technologies implemented in electronics to photonics, certain subfields of nanophotonics can potentially be implemented on-chip, such as topological photonic systems [170], programmable multifunctional nanophotonics [171]. Integrating acousto-optic interactions resulting from stimulated Brillouin scattering has also been explored [172]. Alternatives to conventional and affordable silicon material platform have also been proposed as a method for creating and/or complementing photonic integrated circuits, including InP [173], van der Waals materials [174], photonic crystals [175], and graphene [176].

Prominent developments in on-chip nanophotonics shape global trends and future challenges in the field. In the following subsection, we list some of them.

6.1 Evanescent trap with photonic waveguides

According to recent atomic trap studies, tailored light potentials for atom trapping by evanescent fields from nanofabricated photonic waveguides have the prospect of becoming a central building block in quantum technology devices that are based on ultra-cold atoms. Optical lattices and atom trapping by evanescent fields have already been realized above the glass surface [177], in optical fibers [178],

and in nanowaveguides [179]. However, dense (few tens nanometer between each site) optical lattice with atoms evanescently trapped with nanoscale distance from the waveguide surface of about 50 nm has never been achieved. From the practical point of view, this will allow for intense atom–atom and photon–atom interactions. The waveguides can be integrated on the same chip with other optical elements such as light cavities for atom detection [180], atom manipulation [181], single photon operations [182] and more.

Beside the above-mentioned practical advantages, integrated waveguides have inherent properties which cannot be realized by other atom trapping schemes. For example, compared to atom trapping in optical lattices [128, 183] the separation between adjacent traps can be on subwavelength scales and curved structures can be designed. In comparison to the common atomchip technology which is based on magnetic trapping and guiding by current carrying wires, the atoms are trapped by evanescent homogeneous light fields. This avoids the harmful effects such as fragmentation [184, 185] or reduced lifetime due to technical noise from the current source. The atoms can be brought closer to the chip surface without suffering from Johnson noise generated by the metallic surface [186] and more. A nanowaveguide platform made of Silicon nitride (Si_3N_4) core for collective cold atom–light interaction through evanescent field coupling has been proposed using mirrors [179]. This system, using bi-chromatic evanescent field atom traps, proposes to secure atoms at a minimal distance of 150 nm above the waveguide. A similar system has been proposed [37], as shown in Figure 8f, to use a silicon nitride ridge waveguide with a nano-antenna on top (Figure 8g), in order to trap atoms using an all-dielectric device. For the toroidal nano-antenna, it was shown that the atoms can be trapped at a distance of roughly 70 nm from the surface (Figure 8h).

6.2 Energy-conserving optical elements

One of the greatest challenges in information processing and computing is to reduce the energy consumption not only for the sake of reducing the tremendous amount of electric power used by the computer-based industry, such as Google, Amazon, or Facebook, but also to enable computing devices to operate at a higher frequency without melting as a result of the extra heat. For instance, the cooling all of the world's data centers accounts for 1.5% of total global electricity. It was predicted theoretically that reversible gates may preserve energy together with the data and that reversible devices that may be built entirely with energy-conserving elements [187]. This formalism utilizes linear and nonlinear unitary transformations in relation to conserving optical elements such as optical waveguide based directional couplers.

7 Conclusion

This review showed the rapidly growing on-chip nanophotonics field, including current novel technologies and devices, the challenges and future plans for the research direction in the field. The history of passive optical waveguides and their progress as actual devices such as filters, modulators, detectors, switches, and light sources on a chip, have been reviewed in detail. The far-reaching goal of on-chip nanophotonics is to perform complex tasks within a single chip such as computing, energy conversion, biomedical sensing, and cryptography.

Acknowledgement: This work was supported by Israel Innovation Authority KAMIN program Grant no. 69073. AK is thankful to her students and postdocs whose work occupied large part of this review article: Yakov Greenberg, Pavel Terekhov, Daler Dadadzhanov, Yury Artemyev, Fyodor Morozko, Eran Falek.

References

[1] A. Katiyi and A. Karabchevsky, "Figure of merit of all-dielectric waveguide structures for absorption overtone spectroscopy," *J. Lightw. Technol.*, vol. 35, no. 14, pp. 2902–2908, 2017.
[2] Y. Fang and M. Sun, "Nanoplasmonic waveguides: towards applications in integrated nanophotonic circuits," *Light Sci. Appl.*, vol. 4, no. 6, 2015, e294.
[3] A. Karabchevsky, J. S. Wilkinson, and M. N. Zervas, "Transmittance and surface intensity in 3d composite plasmonic waveguides," *Opt. Express*, vol. 23, no. 11, pp. 14407–14423, 2015.
[4] F. Bernal Arango, A. Kwadrin, and A. F. Koenderink, "Plasmonic antennas hybridized with dielectric waveguides," *ACS Nano*, vol. 6, no. 11, pp. 10156–10167, 2012.
[5] B. Chen, R. Bruck, D. Traviss, et al., "Hybrid photon–plasmon coupling and ultrafast control of nanoantennas on a silicon photonic chip," *Nano Lett.*, vol. 18, no. 1, pp. 610–617, 2018
[6] Y. Galutin, E. Falek, and A. Karabchevsky, "Invisibility cloaking scheme by evanescent fields distortion on composite plasmonic waveguides with si nano-spacer," *Sci. Rep.*, vol. 7, no. 1, p. 12076, 2017.
[7] W. Niu, M. Huang, Z. Xiao, L. Zheng, and J. Yang, "Sensitivity enhancement in TE mode nonlinear planar optical waveguide

sensor with metamaterial layer," *Optik*, vol. 123, no. 6, pp. 547–552, 2012.
[8] D.-K. Qing and G. Chen, "Enhancement of evanescent waves in waveguides using metamaterials of negative permittivity and permeability," *Appl. Phys. Lett.*, vol. 84, no. 5, pp. 669–671, 2004.
[9] V. Ginis, P. Tassin, C. M. Soukoulis, and I. Veretennicoff, "Enhancing optical gradient forces with metamaterials," *Phys. Rev. Lett.*, vol. 110, no. 5, p.057401, 2013.
[10] M. J. Weber, *Handbook of Optical Materials*, Boca Raton, FL, CRC Press, 2018.
[11] M. Born and E. Wolf, *Principles of Optics: Electromagnetic Theory of Propagation, Interference and Diffraction of Light*, London, Elsevier, 2013.
[12] A. M. Urbas, Z. Jacob, L. D. Negro, et al., "Roadmap on optical metamaterials," *J. Opt.*, vol. 18, no. 9, p.093005, 2016.
[13] Y. Xu, Y. Fu, and H. Chen, "Planar gradient metamaterials," *Nat. Rev. Mater.*, vol. 1, no. 12, p. 16067, 2016.
[14] W. C. Chew, E. Michielssen, J. M. Song, and J.-M. Jin, *Fast and Efficient Algorithms in Computational Electromagnetics*, Norwood, MA, Artech House, Inc., 2001.
[15] W. L. Barnes, A. Dereux, and T. W. Ebbesen, "Surface plasmon subwavelength optics," *Nature*, vol. 424, no. 6950, p. 824, 2003.
[16] D. K. Gramotnev and S. I. Bozhevolnyi, "Plasmonics beyond the diffraction limit," *Nat. Photonics*, vol. 4, no. 2, p. 83, 2010.
[17] S. Jahani and Z. Jacob, "All-dielectric metamaterials," *Nat. Nanotechnol.*, vol. 11, no. 1, p. 23, 2016.
[18] N. Yu, P. Genevet, M. A. Kats, et al., "Light propagation with phase discontinuities: generalized laws of reflection and refraction," *Science*, vol. 334, no. 6054, pp. 333–337, 2011.
[19] Q. Wang, E. T. F. Rogers, B. Gholipour, et al., "Optically reconfigurable metasurfaces and photonic devices based on phase change materials," *Nat. Photonics*, vol. 10, no. 1, p. 60, 2016.
[20] A. V. Kildishev, A. Boltasseva, and V. M. Shalaev, "Planar photonics with metasurfaces," *Science*, vol. 339, no. 6125, p. 1232009, 2013.
[21] N. Yu and F. Capasso, "Flat optics with designer metasurfaces," *Nat. Mater.*, vol. 13, no. 2, p. 139, 2014.
[22] N. Engheta and R. W. Ziolkowski, *Metamaterials: Physics and Engineering Explorations*, Hoboken, NJ, John Wiley & Sons, 2006.
[23] A. Karabchevsky, E. Falek, Y. Greenberg, and I. Gurwich, "Broadband transparency with all-dielectric metasurfaces engraved on silicon waveguide facets: effect of inverted and extruded features based on babinet's principle," *Nanoscale Adv.*, 2020, http://dx.doi.org/10.1039/d0na00346h.
[24] V. Pacheco-Peña and N. Engheta, "Antireflection temporal coatings," *Optica*, vol. 7, no. 4, pp. 323–331, 2020.
[25] Y. Greenberg and A. Karabchevsky, "Spatial eigenmodes conversion with metasurfaces engraved in silicon ridge waveguides," *Appl. Opt.*, vol. 58, no. 22, pp. F21–F25, 2019.
[26] A. W. Snyder and J. Love, *Optical Waveguide Theory*, Springer Science & Business Media, 2012.
[27] R. G. Hunsperger, *Integrated Optics: Theory and Technology. Advanced Texts in Physics*, 6th ed. Berlin, Germany, Springer, 2009, Citation Key: hunsperger2009.
[28] L. Chrostowski and M. Hochberg, *Silicon Photonics Design: From Devices to Systems*, Cambridge, Cambridge University Press, 2015.
[29] L. Hagedorn Frandsen, P. Ingo Borel, Y. X. Zhuang, et al., "Ultralow-loss 3-db photonic crystal waveguide splitter," *Optics Lett.*, vol. 29, no. 14, pp. 1623–1625, 2004.
[30] Z. Xiao, X. Luo, P. Huei Lim, et al., "Ultra-compact low loss polarization insensitive silicon waveguide splitter," *Opt. Express*, vol. 21, no. 14, pp. 16331–16336, 2013.
[31] X. Guan, H. Wu, Y. Shi, L. Wosinski, and D. Dai, "Ultracompact and broadband polarization beam splitter utilizing the evanescent coupling between a hybrid plasmonic waveguide and a silicon nanowire," *Opt. Lett.*, vol. 38, no. 16, pp. 3005–3008, 2013.
[32] W. Bogaerts, P. De Heyn, T. Van Vaerenbergh, et al., "Silicon microring resonators," *Laser Photonics Rev.*, vol. 6, no. 1, pp. 47–73, 2012.
[33] V. Govindan and S. Ashkenazi, "Bragg waveguide ultrasound detectors," *IEEE Trans. Ultrason. Ferr. Freq. Control*, vol. 59, no. 10, pp. 2304–2311, 2012.
[34] S. Meister, B. Franke, H. J. Eichler, et al., "Photonic integrated circuits for optical communication: silicon technology enables high complex devices," *Optik Photonik*, vol. 7, no. 2, pp. 59–62, 2012.
[35] Y. Wang, X. Wang, J. Flueckiger, et al., "Focusing sub-wavelength grating couplers with low back reflections for rapid prototyping of silicon photonic circuits," *Opt. Express*, vol. 22, no. 17, pp. 20652–20662, 2014.
[36] A. Dewanjee, J. Stewart Aitchison, and M. Mojahedi, "Experimental demonstration of a high efficiency compact bilayer inverse taper edge coupler for si photonics," *IEEE Photonics Conference (IPC)*, IEEE, 2016, pp. 414–415. 2016.
[37] A. Ang, A. Shalin, and A. Karabchevsky, Optics Letters, 2020, http://dx.doi.org/10.1364/OL.394557.Tailored optical potentials for cs atoms above waveguides with focusing dielectric nano-antenna.
[38] P. T. Lin, S. W. Kwok, H.-Y. G. Lin, et al., "Mid-infrared spectrometer using opto-nanofluidic slot-waveguide for label-free on-chip chemical sensing," *Nano Lett.*, vol. 14, no. 1, pp. 231–238, 2014.
[39] Y. Qian, J. Song, S. Kim, and G. P. Nordin, "Compact 90 trench-based splitter for silicon-on-insulator rib waveguides," *Opt. Express*, vol. 15, no. 25, pp. 16712–16718, 2007.
[40] A. Ghaffari, M. Djavid, and M. Sadegh Abrishamian, "Power splitters with different output power levels based on directional coupling," *Appl. Opt.*, vol. 48, no. 8, pp. 1606–1609, 2009.
[41] A. Katiyi and A. Karabchevsky, "Deflected talbot mediated overtone spectroscopy in near-infrared as a label-free sensor on a chip," *ACS Sensors*, 2020, http://dx.doi.org/10.1021/acssensors.0c00325.
[42] A. Koster, E. Cassan, S. Laval, L. Vivien, and D. Pascal, "Ultracompact splitter for submicrometer silicon-on-insulator rib waveguides," *JOSA A*, vol. 21, no. 11, pp. 2180–2185, 2004.
[43] S. Yang, Y. Zhang, D. W. Grund, et al., "A single adiabatic microring-based laser in 220 nm silicon-on-insulator," *Opt. Express*, vol. 22, no. 1, pp. 1172–1180, 2014.
[44] K. Nemoto, T. Kita, and H. Yamada, "Narrow-spectral-linewidth wavelength-tunable laser diode with si wire waveguide ring resonators," *Appl. Phys. Exp.*, vol. 5, no. 8, 2012, Art No. 082701.

[45] C. T. Phare, Y.-H. D. Lee, J. Cardenas, and M. Lipson, "Graphene electro-optic modulator with 30 ghz bandwidth," *Nat. Photonics*, vol. 9, no. 8, pp. 511–514, 2015.
[46] M. Gould, T. Baehr-Jones, R. Ding, et al., "Silicon-polymer hybrid slot waveguide ring-resonator modulator," *Opt. Express*, vol. 19, no. 5, pp. 3952–3961, 2011.
[47] W. Du, E.-P. Li, and R. Hao, "Tunability analysis of a graphene-embedded ring modulator," *IEEE Photonics Technol. Lett.*, vol. 26, no. 20, pp. 2008–2011, 2014.
[48] A. Nitkowski, L. Chen, and M. Lipson, "Cavity-enhanced on-chip absorption spectroscopy using microring resonators," *Opt. Express*, vol. 16, no. 16, pp. 11930–11936, 2008.
[49] W. W. Shia and R. C. Bailey, "Single domain antibodies for the detection of ricin using silicon photonic microring resonator arrays," *Anal. Chem.*, vol. 85, no. 2, pp. 805–810, 2013.
[50] M. Thiel, G. Flachenecker, and W. Schade, "Femtosecond laser writing of Bragg grating waveguide bundles in bulk glass," *Opt. Lett.*, vol. 40, no. 7, pp. 1266–1269, 2015.
[51] R. G. Krämer, C. Matzdorf, A. Liem, et al., "Femtosecond written fiber Bragg gratings in ytterbium-doped fibers for fiber lasers in the kilowatt regime," *Opt. Lett.*, vol. 44, no. 4, pp. 723–726, 2019.
[52] L. Chen and E. Towe, "Nanowire lasers with distributed-bragg-reflector mirrors," *Appl. Phys. Lett.*, vol. 89, no. 5, 2006, Art no. 053125.
[53] L.-Y. Shao, X. Dong, A. P. Zhang, H.-Y. Tam, and S. He, "High-resolution strain and temperature sensor based on distributed Bragg reflector fiber laser," *IEEE Photonics Technol. Lett.*, vol. 19, no. 20, pp. 1598–1600, 2007.
[54] W. Liang, Y. Huang, Y. Xu, R. K. Lee, and A. Yariv, "Highly sensitive fiber Bragg grating refractive index sensors," *Appl. Phys. Lett.*, vol. 86, no. 15, p. 151122, 2005.
[55] X. Fang, C. R. Liao, and D. N. Wang, "Femtosecond laser fabricated fiber Bragg grating in microfiber for refractive index sensing," *Opt. Lett.*, vol. 35, no. 7, pp. 1007–1009, 2010.
[56] M. Papes, P. Cheben, D. Benedikovic, et al., "Fiber-chip edge coupler with large mode size for silicon photonic wire waveguides," *Opt. Express*, vol. 24, no. 5, pp. 5026–5038, 2016.
[57] J. P. Epping, T. Hellwig, M. Hoekman, et al., "On-chip visible-to-infrared supercontinuum generation with more than 495 thz spectral bandwidth," *Opt. Express*, vol. 23, no. 15, pp. 19596–19604, 2015.
[58] T. Hiraki, T. Aihara, K. Hasebe, et al., "Heterogeneously integrated iii–v/si mos capacitor mach–zehnder modulator," *Nat. Photonics*, vol. 11, no. 8, pp. 482–485, 2017.
[59] C. Scales, I. Breukelaar, and P. Berini, "Surface-plasmon schottky contact detector based on a symmetric metal stripe in silicon," *Opt. Lett.*, vol. 35, no. 4, pp. 529–531, 2010.
[60] T. Yin, R. Cohen, M. M. Morse, G. Sarid, Y. Chetrit, D. Rubin, and M. J. Paniccia, "40gb/s ge-on-soi waveguide photodetectors by selective ge growth," in *OFC/NFOEC 2008-2008 Conference on Optical Fiber Communication/National Fiber Optic Engineers Conference*, IEEE, 2008, pp. 1–3.
[61] X. Liu, M. Pu, B. Zhou, et al., "Octave-spanning supercontinuum generation in a silicon-rich nitride waveguide," *Opt. Lett.*, vol. 41, no. 12, pp. 2719–2722, 2016.
[62] H. Byun, D. Pudo, S. Frolov, et al., "Integrated low-jitter 400-mhz femtosecond waveguide laser," *IEEE Photonics Technol. Lett.*, vol. 21, no. 12, pp. 763–765, 2009.
[63] M. J. R. Heck, A. La Porta, X. J. M. Leijtens, et al., "Monolithic awg-based discretely tunable laser diode with nanosecond switching speed," *IEEE Photonics Technol. Lett.*, vol. 21, no. 13, pp. 905–907, 2009.
[64] R. G. Hunsperger, *Integrated Optics*, vol. 4, Berlin, Springer, 1995.
[65] H. Xu, X. Xiao, X. Li, et al., "High speed silicon mach-zehnder modulator based on interleaved pn junctions," *Opt. Express*, vol. 20, no. 14, pp. 15093–15099, 2012.
[66] G. Li, A. V. Krishnamoorthy, I. Shubin, et al., "Ring resonator modulators in silicon for interchip photonic links," *IEEE J. Sel. Top. Quantum Electron.*, vol. 19, no. 6, pp. 95–113, 2013.
[67] P. Berini, A. Olivieri, and C. Chen, "Thin au surface plasmon waveguide schottky detectors on p-si," *Nanotechnology*, vol. 23, no. 44, p. 444011, 2012.
[68] M. Liu, X. Yin, E. Ulin-Avila, et al., "A graphene-based broadband optical modulator," *Nature*, vol. 474, no. 7349, pp. 64–67, 2011.
[69] M. Romagnoli, V. Sorianello, M. Midrio, et al., "Graphene-based integrated photonics for next-generation datacom and telecom," *Nat. Rev. Mater.*, vol. 3, no. 10, pp. 392–414, 2018.
[70] K. I. Bolotin, K. J. Sikes, Z. Jiang, et al., "Ultrahigh electron mobility in suspended graphene," *Solid State Commun.*, vol. 146, no. 9-10, pp. 351–355, 2008.
[71] A. S. Mayorov, R. V. Gorbachev, S. V. Morozov, et al., "Micrometer-scale ballistic transport in encapsulated graphene at room temperature," *Nano Lett.*, vol. 11, no. 6, pp. 2396–2399, 2011.
[72] K. F. Mak, M. Y. Sfeir, Y. Wu, C. H. Lui, J. A. Misewich, and T. F. Heinz, "Measurement of the optical conductivity of graphene," *Phys. Rev. Lett.*, vol. 101, no. 19, p. 196405, 2008.
[73] S. J. Koester and M. Li, "High-speed waveguide-coupled graphene-on-graphene optical modulators," *Appl. Phys. Lett.*, vol. 100, no. 17, p. 171107, 2012.
[74] S.-W. Ye, F. Yuan, X.-H. Zou, M. K. Shah, R.-G. Lu, and Y. Liu, "High-speed optical phase modulator based on graphene-silicon waveguide," *IEEE J. Sel. Top. Quantum Electron.*, vol. 23, no. 1, pp. 76–80, 2016.
[75] C. A. Zaugg, Z. Sun, V. J. Wittwer, et al., "Ultrafast and widely tuneable vertical-external-cavity surface-emitting laser, mode-locked by a graphene-integrated distributed Bragg reflector," *Opt. Express*, vol. 21, no. 25, pp. 31548–31559, 2013.
[76] A. Karabchevsky and A. V. Kavokin, "Giant absorption of light by molecular vibrations on a chip," *Sci. Rep.*, vol. 6, 2016, https://doi.org/10.1038/srep21201.
[77] A. Karabchevsky, A. Katiyi, M. I. M. Bin Abdul Khudus, and A. V. Kavokin, "Tuning the near-infrared absorption of aromatic amines on tapered fibers sculptured with gold nanoparticles," *ACS Photonics*, vol. 5, no. 6, pp. 2200–2207, 2018.
[78] A. Katiyi and A. Karabchevsky, "Si nanostrip optical waveguide for on-chip broadband molecular overtone spectroscopy in near-infrared," *ACS Sensors*, vol. 3, no. 3, pp. 618–623, 2018.
[79] A. Katiyi, J. Zorea, A. Halstuch, M. Elkabets, and A. Karabchevsky, "Surface roughness-induced absorption acts as an ovarian cancer cells growth sensor-monitor," *Biosens. Bioelectron.*, vol. 161, p. 112240, 2020.
[80] D. R. Dadadzhanov, T. A. Vartanyan, and A. Karabchevsky, "Differential extinction of vibrational molecular overtone transitions with gold nanorods and its role in surface enhanced

near-ir absorption (senira)," *Opt. Express*, vol. 27, no. 21, pp. 29471–29478, 2019.
[81] W. S.Struve, *Fundamentals of Molecular Spectroscopy*, New York, Wiley, 1989.
[82] M. Reichenbächer and J. Popp, *Challenges in Molecular Structure Determination*, Berlin, Germany, Springer Science & Business Media, 2012.
[83] R. Siebert and J. Müller, "Infrared integrated optical evanescent field sensor for gas analysis: part i: system design," *Sens. Actuators. A. Phys.*, vol. 119, no. 1, pp. 138–149, 2005.
[84] P. T. Lin, S. W. Kwok, H.-Y. G. Lin, et al., "Mid-infrared spectrometer using opto-nanofluidic slot-waveguide for label-free on-chip chemical sensing," *Nano Lett.*, vol. 14, no. 1, pp. 231–238, 2013.
[85] P. A. Anderson, B. S. Schmidt, and M. Lipson, "High confinement in silicon slot waveguides with sharp bends," *Opt. Express*, vol. 14, no. 20, pp. 9197–9202, 2006.
[86] J. Grdadolnik, "Atr-ftir spectroscopy: its advantage and limitations," *Acta Chim. Slov.*, vol. 49, no. 3, pp. 631–642, 2002.
[87] Q. Wang and G. Farrell, "All-fiber multimode-interference-based refractometer sensor: proposal and design," *Optics Lett.*, vol. 31, no. 3, pp. 317–319, 2006.
[88] K. Schroeder, W. Ecke, R. Mueller, R. Willsch, and A. Andreev, "A fibre Bragg grating refractometer," *Meas. Sci. Technol.*, vol. 12, no. 7, p. 757, 2001.
[89] O. V. Borovkova, D. O. Ignatyeva, S. K. Sekatskii, A. Karabchevsky, and V. I. Belotelov, "High-q surface electromagnetic wave resonance excitation in magnetophotonic crystals for supersensitive detection of weak light absorption in the near-infrared," *Photonics Res.*, vol. 8, no. 1, pp. 57–64, 2020.
[90] Y. Fang and M. Sun, "Nanoplasmonic waveguides: towards applications in integrated nanophotonic circuits," *Light Sci. Appl.*, vol. 4, no. 6, 2015, e294–e294.
[91] V. Pacheco-Peña, I. V. Minin, O. V. Minin, and M. Beruete, "Increasing surface plasmons propagation via photonic nanojets with periodically spaced 3d dielectric cuboids," *Photonics*, vol. 3, no. 11, p. 10, 2016.
[92] J. Wang, F. Sciarrino, A. Laing, and M. G. Thompson, "Integrated photonic quantum technologies," *Nat. Photonics*, vol. 14, no. 5, pp. 273–284, 2020.
[93] A. Politi, M. J. Cryan, J. G. Rarity, S. Yu, and J. L. O'Brien, "Silica-on-silicon waveguide quantum circuits," *Science*, vol. 320, no. 5876, pp. 646–649, 2008.
[94] J. Claudon, J. Bleuse, N. Singh Malik, et al., "A highly efficient single-photon source based on a quantum dot in a photonic nanowire," *Nat. Photonics*, vol. 4, no. 3, pp. 174–177, 2010.
[95] N. Mizuochi, T. Makino, H. Kato, et al., "Electrically driven single-photon source at room temperature in diamond," *Nat. Photonics*, vol. 6, no. 5, p. 299, 2012.
[96] O. Kahl, S. Ferrari, V. Kovalyuk, G. N. Goltsman, A. Korneev, and W. H. P. Pernice, "Waveguide integrated superconducting single-photon detectors with high internal quantum efficiency at telecom wavelengths," *Sci. Rep.*, vol. 5, p. 10941, 2015.
[97] F. Najafi, J. Mower, N. C. Harris, et al., "On-chip detection of non-classical light by scalable integration of single-photon detectors," *Nat. Commun.*, vol. 6, no. 1, pp. 1–8, 2015.
[98] E. Engin, D. Bonneau, C. M. Natarajan, et al., "Photon pair generation in a silicon micro-ring resonator with reverse bias enhancement," *Opt. Express*, vol. 21, no. 23, p. 27826, 2013.
[99] X. Lu, Q. Li, D. A. Westly, et al., "Chip-integrated visible–telecom entangled photon pair source for quantum communication," *Nat. Phys.*, vol. 15, no. 4, pp. 373–381, 2019.
[100] J. B. Spring, P. L. Mennea, B. J. Metcalf, et al., "Chip-based array of near-identical, pure, heralded single-photon sources," *Optica*, vol. 4, no. 1, p. 90, 2017.
[101] H. Jin, F. M. Liu, P. Xu, et al., "On-chip generation and manipulation of entangled photons based on reconfigurable lithium-niobate waveguide circuits," *Phys. Rev. Lett.*, vol. 113, no. 10, p. 103601, 2014.
[102] R. Horn, P. Abolghasem, B. J. Bijlani, D. Kang, A. S. Helmy, and G. Weihs, "Monolithic source of photon pairs," *Phys. Rev. Lett.*, vol. 108, no. 15, p. 153605, 2012.
[103] M. Arcari, I. Söllner, A. Javadi, et al., "Near-unity coupling efficiency of a quantum emitter to a photonic crystal waveguide," *Phys. Rev. Lett.*, vol. 113, no. 9, 2014, Art no. 093603.
[104] F. Lenzini, B. Haylock, J. C. Loredo, et al., "Active demultiplexing of single photons from a solid-state source," *Laser Photonics Rev.*, vol. 11, no. 3, p. 1600297, 2017.
[105] T. Gerrits, N. Thomas-Peter, J. C. Gates, et al., "On-chip, photon-number-resolving, telecommunication-band detectors for scalable photonic information processing," *Phys. Rev. A*, vol. 84, no. 6, 2011, Art no. 060301.
[106] J. P. Sprengers, A. Gaggero, D. Sahin, et al., "Waveguide superconducting single-photon detectors for integrated quantum photonic circuits," *Appl. Phys. Lett.*, vol. 99, no. 18, p. 181110, 2011.
[107] N. J. D. Martinez, M. Gehl, C. T. Derose, et al., "Single photon detection in a waveguide-coupled ge-on-si lateral avalanche photodiode," *Opt. Express*, vol. 25, no. 14, p. 16130, 2017.
[108] P. Vines, K. Kuzmenko, J. Kirdoda, et al., "High performance planar germanium-on-silicon single-photon avalanche diode detectors," *Nat. Commun.*, vol. 10, no. 1, p. 1086, 2019.
[109] C.-K. Hong, Z.-Y. Ou, and L. Mandel, "Measurement of subpicosecond time intervals between two photons by interference," *Phys. Rev. Lett.*, vol. 59, no. 18, p. 2044, 1987.
[110] M. P. A. Jones, C. J. Vale, D. Sahagun, B. V. Hall, and E. A. Hinds, "Spin coupling between cold atoms and the thermal fluctuations of a metal surface," *Phys. Rev. Lett.*, vol. 91, no. 8, 2003, Art no. 080401.
[111] Y.-j. Lin, I. Teper, C. Chin, and V. Vuletić, "Impact of the casimir-polder potential and johnson noise on bose-einstein condensate stability near surfaces," *Phys. Rev. Lett.*, vol. 92, no. 5, 2004, Art no. 050404.
[112] A. Emmert, A. Lupaşcu, G. Nogues, M. Brune, J.-M. Raimond, and S. Haroche, "Measurement of the trapping lifetime close to a cold metallic surface on a cryogenic atom-chip," *Eur. Phys. J. D*, vol. 51, no. 2, pp. 173–177, 2009.
[113] S. Aigner, L. Della Pietra, Y. Japha, et al., "Long-range order in electronic transport through disordered metal films," *Science*, vol. 319, no. 5867, pp. 1226–1229, 2008.
[114] D. M. Harber, J. M. Obrecht, J. M. McGuirk, and E. A. Cornell, "Measurement of the casimir-polder force through center-of-mass oscillations of a bose-einstein condensate," *Phys. Rev. A*, vol. 72, no. 3, 2005, Art no. 033610.

[115] J. M. Obrecht, R. J. Wild, M. Antezza, L. P. Pitaevskii, S. Stringari, and E. A. Cornell, "Measurement of the temperature dependence of the casimir-polder force," *Phys. Rev. Lett.*, vol. 98, no. 6, 2007, Art no. 063201.
[116] T. A. Pasquini, M. Saba, G.-B. Jo, et al., "Low velocity quantum reflection of bose-einstein condensates," *Phys. Rev. Lett.*, vol. 97, no. 9, 2006, Art no. 093201.
[117] J. Esteve, J.-B. Trebbia, and T. Schumm, "Alain Aspect, Christoph I Westbrook, and Isabelle Bouchoule. Observations of density fluctuations in an elongated bose gas: ideal gas and quasicondensate regimes," *Phys. Rev. Lett.*, vol. 96, no. 13, p. 130403, 2006.
[118] B. Yuen, I. J. M. Barr, J. P. Cotter, E. Butler, and E. A. Hinds, "Enhanced oscillation lifetime of a bose–einstein condensate in the 3d/1d crossover," *N. J. Phys.*, vol. 17, no. 9, 2015, Art no. 093041.
[119] B. Rauer, P. Grišins, I. E. Mazets, et al., "Cooling of a one-dimensional bose gas," *Phys. Rev. Lett.*, vol. 116, no. 3, 2016, Art no. 030402.
[120] S. Hofferberth, I. Lesanovsky, B. Fischer, T. Schumm, and J. Schmiedmayer, "Non-equilibrium coherence dynamics in one-dimensional bose gases," *Nature*, vol. 449, no. 7160, pp. 324–327, 2007.
[121] M. Gring, M. Kuhnert, T. Langen, et al., "Relaxation and prethermalization in an isolated quantum system," *Science*, vol. 337, no. 6100, pp. 1318–1322, 2012.
[122] T. Langen, S. Erne, R. Geiger, et al., "Experimental observation of a generalized Gibbs ensemble," *Science*, vol. 348, no. 6231, pp. 207–211, 2015.
[123] M. F. Riedel, P. Böhi, Y. Li, T. W. Hänsch, A. Sinatra, and P. Treutlein, "Atom-chip-based generation of entanglement for quantum metrology," *Nature*, vol. 464, no. 7292, pp. 1170–1173, 2010.
[124] F. Haas, J. Volz, R. Gehr, J. Reichel, and J. Estève, "Entangled states of more than 40 atoms in an optical fiber cavity," *Science*, vol. 344, no. 6180, pp. 180–183, 2014.
[125] P. Facchi, G. Marmo, and S. Pascazio, "Quantum zeno dynamics and quantum zeno subspaces," 2009. in *Journal of Physics: Conference Series*, Vol. 196, IOP Publishing, p.012017.
[126] K. Maussang, G. E. Marti, T. Schneider, et al., "Enhanced and reduced atom number fluctuations in a bec splitter," *Phys. Rev. Lett.*, vol. 105, no. 8, 2010, Art no. 080403.
[127] M. Keil, O. Amit, S. Zhou, D. Groswasser, Y. Japha, and R. Folman, "Fifteen years of cold matter on the atom chip: promise, realizations, and prospects," *J. Mod. Opt.*, vol. 63, no. 18, pp. 1840–1885, 2016.
[128] W. S. Bakr, A. Peng, M. E. Tai, et al., "Probing the superfluid–to–mott insulator transition at the single-atom level," *Science*, vol. 329, no. 5991, pp. 547–550, 2010.
[129] M. Endres, T. Fukuhara, D. Pekker, et al., "The 'higgs' amplitude mode at the two-dimensional superfluid/mott insulator transition," *Nature*, vol. 487, no. 7408, pp. 454–458, 2012.
[130] V. Galitski and I. B. Spielman, "Spin–orbit coupling in quantum gases," *Nature*, vol. 494, no. 7435, pp. 49–54, 2013.
[131] M. C. Beeler, R. A. Williams, K. Jimenez-Garcia, L. J. LeBlanc, A. R. Perry, and I. B. Spielman, "The spin hall effect in a quantum gas," *Nature*, vol. 498, no. 7453, pp. 201–204, 2013.
[132] T. Kimura, Y. Nambu, T. Hatanaka, A. Tomita, H. Kosaka, and K. Nakamura, "Single-photon interference over 150 km transmission using silica-based integrated-optic interferometers for quantum cryptography," *Jpn. J. Appl. Phys.*, vol. 43, no. 9A, p. L1217, 2004.
[133] G. D. Maxwell, P. Townsend, K. Lear, M. Harlow, and R. Cecil, "The use of planar silica waveguide technology in quantum cryptography systems," in *Technical Digest. CLEO/Pacific Rim'99. Pacific Rim Conference on Lasers and Electro-Optics (Cat. No. 99TH8464)*, Vol. 3, IEEE , 1999, pp. 589–590.
[134] A. A. Zyablovsky, A. P. Vinogradov, A. Aleksandrovich Pukhov, A. Viktorovich Dorofeenko, and A. A. Lisyansky, "PT-symmetry in optics," *Physics-Uspekhi*, vol. 57, no. 11, p. 1063, 2014.
[135] C. E. Rüter, K. G. Makris, R. El-Ganainy, D. N. Christodoulides, M. Segev, and D. Kip, "Observation of parity–time symmetry in optics," *Nat. Phys.*, vol. 6, no. 3, pp. 192–195, 2010.
[136] L. Feng, Y.-L. Xu, W. S. Fegadolli, et al., "Experimental demonstration of a unidirectional reflectionless parity-time metamaterial at optical frequencies," *Nat. Mater.*, vol. 12, no. 2, pp. 108–113, 2013.
[137] M. Kremer, T. Biesenthal, L. J. Maczewsky, M. Heinrich, R. Thomale, and A. Szameit, "Demonstration of a two-dimensional PT-symmetric crystal," *Nat. Commun.*, vol. 10, no. 1, p. 435, 2019.
[138] F. Morozko, A. Novitsky, and A. Karabchevsky. Modal purcell factor in PT-symmetric waveguides. arXiv preprint arXiv: 2003.05701, 2020.
[139] H. Hodaei, A. U. Hassan, S. Wittek, et al., "Enhanced sensitivity at higher-order exceptional points," *Nature*, vol. 548, no. 7666, pp. 187–191, 2017.
[140] W. Chen, Ş. Kaya Özdemir, G. Zhao, J. Wiersig, and L. Yang, "Exceptional points enhance sensing in an optical microcavity," *Nature*, vol. 548, no. 7666, pp. 192–196, 2017.
[141] Y. Sun, W. Tan, H.-q. Li, J. Li, and H. Chen, "Experimental demonstration of a coherent perfect absorber with pt phase transition," *Phys. Rev. Lett.*, vol. 112, p. 143903, 2014.
[142] Z. J. Wong, Y.-L. Xu, J. Kim, et al., "Lasing and anti-lasing in a single cavity," *Nat. Photonics*, vol. 10, no. 12, pp. 796–801, 2016.
[143] E. Purcell, "Proceedings of the American Physical Society," *Phys. Rev.*, vol. 69, nos. 11–12, pp. 674–674, 1946.
[144] S. V. Gaponenko, *Introduction to Nanophotonics*, Cambridge, Cambridge University Press, 1988.
[145] V. V. Klimov, M. Ducloy, and V. S. Letokhov, "Spontaneous emission of an atom in the presence of nanobodies," *Quantum Electron.*, vol. 31, no. 7, p. 569, 2001.
[146] S. Hughes, "Enhanced single-photon emission from quantum dots in photonic crystal waveguides and nanocavities," *Opt. Lett.*, vol. 29, no. 22, pp. 2659–2661, 2004.
[147] P. Anger, P. Bharadwaj, and L. Novotny, "Enhancement and quenching of single-molecule fluorescence," *Phys. Rev. Lett.*, vol. 96, no. 11, p. 113002, 2006.
[148] P. Kolchin, N. Pholchai, M. H. Mikkelsen, et al., "High Purcell factor due to coupling of a single emitter to a dielectric slot waveguide," *Nano Lett.*, vol. 15, no. 1, pp. 464–468, 2015.
[149] A. Karabchevsky, A. Mosayyebi, and A. V. Kavokin, "Tuning the chemiluminescence of a luminol flow using plasmonic nanoparticles," *Light Sci. Appl.*, vol. 5, no. 11, p. e16164–e16164, 2016.
[150] Y. Su, P. Chang, C. Lin, and A. S. Helmy, "Record Purcell factors in ultracompact hybrid plasmonic ring resonators," *Sci. Adv.*, vol. 5, no. 8, 2019, https://doi.org/10.1126/sciadv.aav1790.

[151] A. Akbarzadeh, M. Kafesaki, E. N. Economou, C. M. Soukoulis, and J. A. Crosse, "Spontaneous-relaxation-rate suppression in cavities with PT symmetry," *Phys. Rev. A*, vol. 99, no. 3, 2019, https://doi.org/10.1103/physreva.99.033853.
[152] A. Pick, B. Zhen, O. D. Miller, et al., "General theory of spontaneous emission near exceptional points," *Opt. Express*, vol. 25, no. 11, pp. 12325–12348, 2017.
[153] A. Taflove, A. Oskooi, and S. G. Johnson, Eds. Advances in FDTD Computational Electrodynamics: Photonics and Nanotechnology, Boston, Artech House, 2013.
[154] L. Novotny and B. Hecht, *Principles of Nano-Optics*, 2nd ed. Cambridge, Cambridge University Press, 2012.
[155] M. S. Tomaš and Z. Lenac, "Decay of excited molecules in absorbing planar cavities," *Phys. Rev. A*, vol. 56, no. 5, pp. 4197–4206, 1997.
[156] S. I. Maslovski and C. R. Simovski, "Purcell factor and local intensity enhancement in surface-enhanced Raman scattering," *Nanophotonics*, vol. 8, p. 429, 2019.
[157] J. Gao, W. Wang, and X. Yang, "Scaling law of Purcell factor in hyperbolic metamaterial cavities with dipole excitation," *Opt. Lett.*, vol. 44, p. 471, 2019.
[158] K. A. Ivanov, A. R. Gubaidullin, K. M. Morozov, M. E. Sasin, and M. A. Kaliteevskii, "Analysis of the Purcell effect in the waveguide mode by S-quantization," *Opt. Spectrosc.*, vol. 122, no. 5, pp. 835–842, 2017.
[159] K. M. Schulz, D. Jalas, A. Y. Petrov, and M. Eich. "Reciprocity approach for calculating the Purcell effect for emission into an open optical system." *Opt. Express*, Vol. 26, no. 15, pp. 19247–19258, 2018.
[160] X. Zhang and Z. Liu, "Superlenses to overcome the diffraction limit," *Nat. Mater.*, vol. 7, no. 6, p. 435, 2008.
[161] L. Caspani, R. P. M. Kaipurath, M. Clerici, et al., "Enhanced nonlinear refractive index in ε-near-zero materials," *Phys. Rev. Lett.*, vol. 116, no. 23, p. 233901, 2016.
[162] A. Karabchevsky, "On-chip optical vortex-based nanophotonic detectors," *Light Sci. Appl.*, 2020. https://doi.org/10.1038/s41377-020-00359-8.
[163] J. F. Nye and M.V. Berry, "Dislocations in wave trains," *Proc. R. Soc. A Math. Phy.*, vol. 336, no. 1605, pp. 165–190, 1974.
[164] F. Feng, G. Si, C. Min, X. Yuan, and M. Somekh, "On-chip plasmonic spinhall nanograting for simultaneously detecting phase and polarization singularities," *Light Sci. Appl.*, vol. 9, no. 1, pp. 1–9, 2020.
[165] S. Li, Y. Ding, X. Guan, et al., "Compact high-efficiency vortex beam emitter based on a silicon photonics micro-ring," *Optics Lett.*, vol. 43, no. 6, pp. 1319–1322, 2018.
[166] P. D. Terekhov, K. V. Baryshnikova, Y. A. Artemyev, A. Karabchevsky, A. S. Shalin, and A. B. Evlyukhin, "Multipolar response of nonspherical silicon nanoparticles in the visible and near-infrared spectral ranges," *Phys. Rev. B*, vol. 96, no. 3, 2017, Art no. 035443.
[167] P. D. Terekhov, H. K. Shamkhi, E. A. Gurvitz, et al., "Broadband forward scattering from dielectric cubic nanoantenna in lossless media," *Optics Express*, vol. 27, no. 8, pp. 10924–10935, 2019.
[168] P. D. Terekhov, A. B. Evlyukhin, D. Redka, V. S. Volkov, A. S. Shalin, and A. Karabchevsky, "Magnetic octupole response of dielectric quadrumers," *Laser Photonics Rev.*, vol. 14, no. 4, p. 1900331, 2020.
[169] H. K. Shamkhi, K. V. Baryshnikova, A. Sayanskiy, et al., "Transverse scattering and generalized Kerker effects in all dielectric Mie-resonant meta optics," *Phys. Rev. Lett.*, vol. 122, no. 19, p. 193905, 2019.
[170] M. S. Rider, S. J. Palmer, S. R. Pocock, X. Xiao, P. Arroyo Huidobro, and V. Giannini, "A perspective on topological nanophotonics: current status and future challenges," *J. Appl. Phys.*, vol. 125, no. 12, p. 120901, 2019.
[171] D. Pérez, I. Gasulla, and J. Capmany, "Programmable multifunctional integrated nanophotonics," *Nanophotonics*, vol. 7, no. 8, pp. 1351–1371, 2018.
[172] B. J. Eggleton, C. G. Poulton, P. T. Rakich, M. J. Steel, and G. Bahl, "Brillouin integrated photonics," *Nat. Photonics*, vol. 13, no. 10, pp. 664–677, 2019.
[173] M. Smit, K. Williams, and J. van der Tol, "Past, present, and future of InP-based photonic integration," *APL Photonics*, vol. 4, no. 5, 2019, Art no. 050901.
[174] C.-h. Liu, J. Zheng, Y. Chen, T. Fryett, and A. Majumdar, "Van der Waals materials integrated nanophotonic devices [Invited]," *Opt. Mater. Express*, vol. 9, no. 2, pp. 384–399, 2019.
[175] M. Notomi and T. Sogawa, "Nanophotonic technologies for on-chip photonic integration," *NTT Technical Rev.*, vol. 16, no. 7, p. 7, 2018.
[176] M. Romagnoli, V. Sorianello, M. Midrio, et al., "Graphene-based integrated photonics for next-generation datacom and telecom," *Nat. Rev. Mater.*, vol. 3, no. 1010, pp. 392–414, 2018.
[177] Y. B. Ovchinnikov, S. V. Shul'ga, and V. I. Balykin, "An atomic trap based on evanescent light waves," *J. Phys. B*, vol. 24, no. 14, p. 3173, 1991.
[178] E. Vetsch, D. Reitz, G. Sagué, R. Schmidt, S. T. Dawkins, and A. Rauschenbeutel, "Optical interface created by laser-cooled atoms trapped in the evanescent field surrounding an optical nanofiber," *Phys. Rev. Lett.*, vol. 104, no. 20, p. 203603, 2010.
[179] Y. Meng, J. Lee, M. Dagenais, and S. L. Rolston, "A nanowaveguide platform for collective atom-light interaction," *Appl. Phys. Lett.*, vol. 107, no. 9, 2015, Art no. 091110.
[180] T. Aoki, B. Dayan, E. Wilcut, et al., "Observation of strong coupling between one atom and a monolithic microresonator," *Nature*, vol. 443, no. 7112, pp. 671–674, 2006.
[181] J. Volz, R. Gehr, G. Dubois, J. Estève, and J. Reichel, "Measurement of the internal state of a single atom without energy exchange," *Nature*, vol. 475, no. 7355, pp. 210–213, 2011.
[182] S. Rosenblum, O. Bechler, I. Shomroni, Y. Lovsky, G. Guendelman, and B. Dayan, "Extraction of a single photon from an optical pulse," *Nat. Photonics*, vol. 10, no. 1, pp. 19–22, 2016.
[183] E. Haller, J. Hudson, A. Kelly, et al., "Single-atom imaging of fermions in a quantum-gas microscope," *Nat. Phys.*, vol. 11, no. 9, pp. 738–742, 2015.
[184] M. P. A. Jones, C. J. Vale, D. Sahagun, et al., "Cold atoms probe the magnetic field near a wire," *J. Phys. B*, vol. 37, no. 2, p. L15, 2003.
[185] T. Schumm, J. Estève, C. Figl, et al., "Atom chips in the real world: the effects of wire corrugation," *Eur. Phys. J. D*, vol. 32, no. 2, pp. 171–180, 2005.
[186] C. Henkel, P. Krüger, R. Folman, and J. Schmiedmayer, "Fundamental limits for coherent manipulation on atom chips," *Appl. Phys. B*, vol. 76, no. 2, pp. 173–182, 2003.
[187] E. Cohen, S. Dolev, and M. Rosenblit, "All-optical design for inherently energy-conserving reversible gates and circuits," *Nat. Commun.*, vol. 7, no. 1, pp. 1–8, 2016.